Geo-thermochronological analysis reveals transition from transverse to axial detrital inputs during Cretaceous rifting in the Songliao Basin, NE China

Nan Wang[a,b,c], Zhiyong Zhang[a]*, Marco G. Malusà[c]*, Jien Zhang[a], Lin Wu[a], Dunfeng Xiang[a,b], Wenjiao Xiao[d]

[a]State Key Laboratory of Lithospheric Evolution, Institute of Geology and Geophysics, Chinese Academy of Sciences, Beijing 100029, China

[b]University of Chinese Academy of Sciences, Beijing 100049, China

[c]Department of Earth and Environmental Sciences, University of Milano-Bicocca, Milano 20126, Italy

[d]Xinjiang Research Center for Mineral Resources, Xinjiang Institute of Ecology and Geography, Chinese Academy of Sciences, Urumqi 830011, China

*Corresponding author: Zhiyong Zhang.

E-mail: zyzhang@mail.iggcas.ac.cn, zhang.nju@gmail.com

Telephone: +86 10 82998477.

*Corresponding author: Marco G. Malusà

E-mail: marco.malusa@unimib.it.

Telephone: +39 02 6448 2065.

Running Head

Transition from transverse to axial detrital inputs in the Songliao Basin

Significance Statement

This manuscript presents new geo-thermochronological dataset of northeastern Songliao Basin in NE China, and discusses the drainage and sedimentation patterns within the framework of published geochronology dataset. Our results show that tectonic extension and volcanism controlled the Songliao Basin sedimentation pattern during the syn-rift stage at ~118–103 Ma, but the thermal subsidence and southern source uplift for the post-rift stage at ~103–91 Ma, with the provenance change and drainage reorganization.

Abstract

The impact of tectonics, volcanism and climate in controlling temporal and spatial variations in rift basin sedimentation is still poorly understood. Here, we tackle this issue by the analysis of mid-Cretaceous sediments deposited in the Songliao Basin, northeastern China. We present new zircon U-Pb, apatite fission-track and trace-element data from the northeastern part of the basin, which are discussed within the framework of published geochronology dataset. Our results reveal a major provenance change from syn-rift tectonic extension to post-rift thermal subsidence at ~103 Ma. During the syn-rift stage, the detrital inputs were dominantly from transverse rivers sourced from the surrounding mountains including graben shoulders and volcanoes. During the post-rift stage and coeval thermal subsidence, the basin sedimentation was controlled by coexisting transverse and axial drainage systems sourced from uplifting regions in the south. We conclude that tectonics, not climate, exerted a major control in sediment provenance change in the mid-Cretaceous Songliao Basin.

1. INTRODUCTION

Rift-basin drainage and sedimentation patterns have been extensively studied worldwide (Frostick & Reid, 1989, 1990; Khalil & McClay, 2009; Muravchik et al., 2017; Olierook et al., 2019;

Tiercelin, 1990) and are considered to be closely linked to tectonics, climate and volcanism (Chen et al., 2022; Gawthorpe & Leeder, 2000; Lambiase & Bosworth, 1995; Tiercelin, 1990). Many authors indicate tectonics as the primary control on drainage pattern and sedimentation (e.g., Olierook et al., 2019), other underline the effects of volcanism (Chen et al., 2022; Elia et al., 2016), whereas other authors emphasize the impact of climate (Lambiase & Bosworth, 1995; Teixeira et al., 2018) and associated changes in precipitation patterns that induce changes in erosion rate, accumulation rate and sediment provenance (Goddard & Carrapa, 2018; Jepson et al., 2021; Teixeira et al., 2018). Due to the complexity of tectonics, climate and volcanism interplay during rift-basin evolution, understanding the spatial and temporal interactions among these factors remains challenging.

The Songliao basin, located in northeastern China, is one of the major late Mesozoic intra-continental rift basins of the eastern Asia continental margin (Figure 1; Wang et al., 2016b). It experienced a Late Jurassic–Early Cretaceous syn-rift stage and a Late Cretaceous post-rift stage, with the formation of two sets of NNE and NW fault systems controlling the boundaries of the graben basins (Li et al., 2021b; Wang et al., 2016b, 2021). Previous works was mainly focused on the Late Cretaceous provenance and drainage patterns (e.g., Li et al., 2021b; Song et al., 2022; Zhang et al., 2017a, b; Zhao et al., 2013), with limited research work on the Early–mid Cretaceous basin evolution. This study is focused on the reconstruction of the drainage evolution during the mid-Cretaceous syn-rift and post-rift stages of the Songliao basin. Our results, when combined with published paleo-climate evolution indicators, shed light on the relationships between tectonics, climate and volcanism during rifting.

2. GEOLOGICAL BACKGROUND

2.1 Regional setting

The evolution of northeastern Asia is intimately linked to the subduction of the Paleo-Pacific Plate (Figure 1; Liu et al., 2020a; Wu et al., 2021). The region experienced a tectonic transition from Early Cretaceous extension, with the development of half-graben basins (e.g., Wang et al., 2016b; Zhang et al., 2017b) and extensive magmatism (e.g., Wu et al., 2011; Xu et al., 2013), to Late Cretaceous periodical compression leading to basin inversion (e.g., Li et al., 2021b; Pang et al., 2020; Suo et al., 2020; Zhang et al., 2017b). The Songliao Basin, located along the Late Mesozoic active continental margin of the Paleo-Pacific subduction zone, evolved from a former Triassic–Middle Jurassic foreland basin (Li et al., 2021b) to become a mega-rift system during the Early Cretaceous (e.g., Ge et al., 2012; Wang et al., 2016b) and be later affected by thermal subsidence during the Late Cretaceous (Wang et al., 2016b; Zhang et al., 2017b).

2.2 The Songliao basin stratigraphic succession

The Lower Cretaceous succession of the basin, mainly distributed in the grabens related to the syn-rift stage, includes the Shahezi Fm. (K_1s) and the Yingcheng Fm. (K_1y) (Figures 2, 3 and S2). The Shahezi Fm. consists of conglomerates, sandstones and mudstones with interbedded coal seams and volcanic rocks (Figure S2; Li et al., 2021b). The unconformably overlying Yingcheng Fm. records a late Early Cretaceous volcanic cycle and mainly consists of volcanic and volcaniclastic rocks with minor lacustrine facies (Figure S2; e.g., Li et al., 2021b; Wang et al., 2016b).

The Upper Cretaceous post-rift succession includes the Denglouku Fm. (K_2d) and the Quantou Fm. (K_2q) (Figure S2). The former contains conglomerates in the lower part and varicolored siltstone and mudstone intercalated with sandstone and coal seams (Figure S2; Wang et al., 2016b). The latter

includes coarse-grained red beds intercalated with fluviatile purple-dark mudstones (Figure S2; Li et al., 2021b; Wang et al., 2016b).

2.3 Potential provenance U-Pb and fission-track signals for the Cretaceous Songliao Basin

The Songliao basin is surrounded by potential sources of detritus with distinguishable geo-thermochronologic fingerprints: the Zhangguangcai Range in the east, the Lesser Xing'an Range in the north, the Great Xing'an Range in the west, and the northern margin of the North China Craton in the south (Figure 1; Wu et al., 2011).

The Zhangguangcai Range is mainly composed of Upper Triassic–Middle Jurassic granites and minor Paleozoic granites (Liu et al., 2008; Wu et al., 2011; Xu et al., 2013), with dominant zircon U-Pb ages at ~210–170 Ma (Figures 1 and S1) and apatite fission-track ages at ~150 Ma (Figure 1). The Lesser Xing'an Range is dominated by two main stages of magmatism of Cambrian–Ordovician (~510–450 Ma) and Late Triassic–Middle Jurassic age (~210–170 Ma; Figure 1), and apatite fission-track ages peaking at ~65 Ma (Figure 1). Early Cretaceous volcanism (~150–110 Ma, peaking at ~130 Ma) is widespread and appears over a vast area throughout the Great Xing'an Range (Figure 1; Xu et al., 2013; Zhang et al., 2010), where minor amounts of granitoids were already emplaced during the Early Paleozoic (~500–460 Ma), Carboniferous–Permian (~350–250 Ma), Jurassic (~190–160 Ma) and Early Cretaceous (~145–120 Ma; Figure 1; Wu et al., 2011). Apatite fission-track data peak at ~55 Ma (Figure 1).

The Yanshan Fold Belt and Liao-Ji Region are located along the northern margin of the eastern North China Craton (Figure 1; Wang et al., 2023). The former dominantly consists of Precambrian basement rocks, Lower Permian–Middle Triassic igneous rocks, and Lower Jurassic to Lower Cretaceous magmatic rocks yielding zircon U-Pb ages of ~2.5 Ga, ~1.6–1.8 Ga, ~260–240 Ma, ~162

Ma and ~128 Ma (Figure 1). The latter is dominated by Precambrian basement rocks, Upper Permian–Jurassic and Lower Cretaceous magmatic rocks with zircon U-Pb ages of ~2.5 Ga, ~2.2 Ga, ~1.8 Ga, ~260–150 Ma and ~140–110 Ma (Figure 1). In the basement underneath the Songliao basin, Triassic strata and plutons yield zircon U-Pb ages peaking at ~270–230 Ma and ~170–160 Ma (Figure 1).

3. SAMPLING, ANALYTICAL METHODS AND DATA COMPILATION

Eighteen samples, including sixteen sandstone and two volcanic rock samples, were collected from the Binxian Graben for this study (Figures 1, 2, S1 and S2; Table S1). Samples B1–B8, B12–B16 and B9–B11 are from the Quantou, Denglouku and Yingcheng Fms. respectively, whereas samples B17–B18 are from the Jurassic Ningyuancun Fm. (Figure S1; Table S1). Ten samples were selected and processed for zircon U-Pb analysis and seven samples for apatite fission-track and trace-element analyses (Tables S1 and S2). The detailed sample information, analytical procedures and result descriptions are shown in the Supporting Information and Supplementary Tables 1, 2 and 3.

Previously published detrital zircon U-Pb data, together with our new data from the Songliao Basin (3199 analyses with <10% discordance from 49 samples), were compiled in Figure 2. These samples are from the syn-rift to post-rift successions exposed in the eastern Songliao Basin (Figure 2). Samples S4, S18, S21 and S25 belong to volcanic-sedimentary successions, whereas the other samples are from sandstones and conglomerates (detailed information in Table S3).

4. RESULTS

4.1 Syn-rift stage (Shahezi and Yingcheng Fms., ~118–103 Ma)

Samples S22 and S25–S32 from the south uplift region and the Xujiaweizi Graben (Figure 2)

are dominated by late Early Cretaceous (~120–110 Ma) magmatic zircon grains, accounting for >50% of the grain-age distributions, with two secondary age groups at ~190–150 Ma and ~250–210 Ma and a minor one at ~330–280 Ma (Figure 2; An, 2018; Cheng, 2019; Song et al., 2022; Yu et al., 2020), whose major provenance could be derived from the recycling of coeval volcanogenic successions deposited at the rift shoulders (Figures 1, 2, 3c and S10). In the Changling and Lishu Grabens (S23 and S24), the dominant age groups at ~280–240 Ma and ~200–160 Ma are likely sourced from the erosion or recycling of the Songliao Basin basement (including plutons and Triassic strata; Figures 1, 2 and S10). The zircon U-Pb, Hf isotope, apatite fission-track and trace-element data from the grabens in the eastern basin margin (S20 and S21) attest to provenance from ~200–170 Ma juvenile magmatic rocks found in the Zhangguangcai Range and Liao-Ji Region (Figures 1, 2, 3e and S6–10; Song et al., 2022).

4.2 Post-rift stage (Denglouku and Quantou Fms., ~103–91 Ma)

Zircon U-Pb data from the southeastern basin margin (S5, S6, S12, S13) indicate detritus derived from the Liao-Ji Region, with appearance of Precambrian zircon grains in the Denglouku Fm., which further increase in the Quantou Fm. (Figures 1, 2 and S10; Li et al., 2012, 2020). Major sediment supply in the northeastern basin margin (S1–4, S14–15) was still from the Zhangguangcai Range (Figures 1, 2 and S10), however, the occurrence of minor age group at ~240–210 Ma in the Quantou Fm. (S1 and S2) possibly indicates some detrital input from southern sources (Figures 1 and 2), as confirmed by the occurrence of apatite grains with large D_{par} values (S2, Figure S9).

Three samples from the lower Denglouku Fm. (S19) and upper Quantou Fm. (S7 and S8) in the southern Songliao Basin show a remarkable provenance change from south Great Xing'an Range to Liao-Ji Region and/or Yanshan Fold Belt (Figures 1, 2 and S10; Wang et al., 2022a). Four samples

from the 2nd, 3rd and 4th member of Denglouku Fm. (S16, S17, S18) and Quantou Fm. (S9) in the north graben region indicate gradually increasing proportions of zircon U-Pb ages at ~150–140 Ma, ~320–240 Ma, ~1.8 Ga and ~2.5 Ga, possibly derived from the Liao-Ji Region and/or Yanshan Fold Belt, and decreasing proportions of zircon U-Pb ages at ~130–110 Ma and ~170 Ma, possibly sourced mainly from the Great Xing'an Range and Zhangguangcai Range (Figures 1, 2 and S10). The dominance of ~130–120 Ma zircon grains in samples S10 and S11 (Quantou Fm.) that are proximal to the graben margin indicate detritus shed from the Great Xing'an Range (Figures 1, 2 and S10).

5. DISCUSSION AND CONCLUSION

During the syn-rift stage, there are considerable differences in detrital zircon spectra of coeval sediment samples collected from different grabens of the Songliao basin (Figure 2). This observation implies the lack of an axial drainage system across the basin (Figure 4a), which was precluded by the presence of along-strike barriers formed by accommodation zones with positive topographic features (Lambiase & Bosworth, 1995). The accommodation zones segmented the rift system into grabens with depocenters isolated from each other and no sediment connection (Figures 4a and S11–S14; Lambiase & Bosworth, 1995). Besides, volcanoes located in rift topographic lows (Wang et al., 2016a, b) could also locally block any potential axial fluvial systems, thus creating isolated lakes and depocenters (Chen et al., 2022), but also significantly increasing the accumulation rate (Figure 3b). The drainage geometry in these isolated grabens characterized the limited fan delta-lacustrine-volcanic system (Figures S11 and S12; Table S4). During tectonic extension, subsidence rate is generally greater than detritus input, creating accommodation space and promoting the development of scarps on the rift shoulders (Olierook et al., 2019). In the Songliao basin, the

detritus derived from the surrounding mountains and/or prominent footwall escarpments were transported by the transverse drainage towards the graben depocenters (Figures 4a and S12).

Transition from tectonic extension to thermal subsidence took place in the middle Cretaceous at ca. 103 Ma (Ge et al., 2012; Wang et al., 2016b). Collectively, the graben margins were still controlled by transverse drainage at this time (Figure 4b), and the areas more proximal to the rift axis in the north were affected sporadically by an axial drainage, with detritus from the Liao-Ji Region transported to the north basin since the middle Cretaceous (upper Denglouku Fm.; Figure 4b). Transition from dominant fan delta-lacustrine-volcanic facies deposited in the grabens, to alluvial fan-alluvial plain-lacustrine facies (Denglouku Fm.) and fluvial-floodplain-shallow lake facies across the entire basin (Quantou Fm.; Figures S11–15; Table S4; Feng et al., 2010; Yang et al., 2021), also points to a notable drainage reorganization in mid Cretaceous times.

Thermal-subsidence periods are typically characterized by equilibrium between generation of long-wavelength accommodation space and sediment supply, which would promote axial drainage development and incorporation of materials from distal sources (Friedmann & Burbank, 1995; Gawthorpe & Leeder, 2000; Olierook et al., 2019). Besides, mountain uplifting could be another important player leading to basin drainage reorganization, as attested in the Songliao Basin by depocenter migration towards the northwest (Zhang et al., 2017b), and by thermochronological evidence of detrital supply from southern sources (Figure S16). This is also consistent with the occurrence of high-elevation coastal mountains along the eastern Asian margin during the early Late Cretaceous (Zhang et al., 2016, 2021). This suggests that tectonics promoting mountain uplift coupled with thermal subsidence in the basin favored the establishment of an axial northward-directed transport of detritus (Figure 4b).

Climate is another important factor generally affecting erosion and accumulation rates. Humid climate with high precipitation amplifies tectonic signals by increasing erosion rates recorded in sedimentary successions, whereas arid climate inhibits erosion thus masking any contemporaneous tectonic signals (e.g., Goddard & Carrapa, 2018; Jepson et al., 2021). There is a pronounced climate variation recorded from the lower Denglouku Fm., associated with a humid and relatively high temperature climate, to the upper Denglouku and Quantou Fms. associated with dry and cold climate (Figure 3d). However, the steadily increasing accumulation rate documented through the Denglouku and Quantou Fms. (Figure 3b) suggests that the effects of climate are less important than tectonics and volcanism in shaping the evolution of the basin.

In summary: (i) During the Songliao basin syn-rift stage, the fault-bounded graben basin sedimentation was controlled by tectonic extension and volcanism, and detritus input from the surrounding mountains, including graben shoulders and volcanoes, were transported by the transverse drainage systems into the basin; (ii) During the post-rift stage, the basin sedimentation was controlled by thermal subsidence and uplift of southern source area, with consequent drainage reorganization and provenance changes with the development of an axial drainage system.

ACKNOWLEDGEMENTS

This work was supported by the National Natural Science Foundation of China (grant numbers 41888101, 42230303 and 92055213). Scientific Editor Carlo Doglioni, Associate Editor Vincenzo Stagno, and two anonymous are appreciated for their insightful comments.

FIGURE 1

(a) Schematic diagram showing the relative contributions between rift axially-derived and shoulder-derived detritus. (b) Schematic tectonic subdivision of the Eurasian continent, modified

after Liu et al. (2017). (c) Topographic map of the northeast China, showing the location of the Songliao basin and surrounding mountain ranges. (d) Zircon U-Pb and AFT kernel density estimations (KDE) from different potential provenances surrounding the Songliao Basin. Abbreviations: YSFB–Yanshan Fold Belt; SGXR–South Great Xing'an Range; NGXR–Nouth Great Xing'an Range; LXR–Lesser Xing'an Range; ZGR–Zhangguangcai Range; SB–Songliao Basin; LJR–Liao-Ji Region. References and data related to zircon U-Pb data and apatite fission track of the Songliao basin and surrounding mountains are presented in the Supporting Information or refer to Ma and Xu (2021); Wu et al. (2011); Zhang et al. (2014), and Supplementary Tables 4, 5, and 7.

FIGURE 2

Summarized detrital zircon U-Pb KDEs or PDPs from the Shahezi, Yingcheng, Denglouku and Quantou Fms. in the Songliao Basin (An, 2018; Cheng, 2019; Li et al., 2012, 2020, 2021a; Liu, 2020b; Song et al., 2022; Wang et al., 2022a; Yang et al., 2014; Yu et al., 2020; Zhang et al., 2017b; Zhang, 2018, and this study). The Songliao basin map showing Lower Cretaceous segmented volcanogenic grabens (in pink), which is covered by the basin-wide post-rift sedimentary sequence of the Upper Cretaceous (white), modified after Wang et al. (2016). Sample locations are also indicated in this map. Detailed zircon U-Pb and Hf isotope, apatite fission track and trace element compositions description and data see in the Supporting Information and Supplementary Table 6. Abbreviations: YSFB–Yanshan Fold Belt; GXR–Great Xing'an Range; LXR–Lesser Xing'an Range; ZGR–Zhangguangcai Range; SBB–Songliao Basin Basement (including Triassic strata and plutons); LJR–Liao-Ji Region.

FIGURE 3

(a) The depositional age constraints of the Shahezi, Yingcheng, Denglouku and Quantou Fms..

References: a–An (2018); b–Yu et al. (2020); c–Liu et al. (2021); d–Wang et al. (2022b); e–Ma et al. (2020). (b) Accumulation rate estimated by the depositional age constrains and thickness from the SK2E well. It shows the steadily increasing accumulation rate from the Denglouku Fm. to Quantou Fm.. (c) The summarized zircon U-Pb ages from late Early Cretaceous volcanic rocks deposited in the Songliao Basin (Data see in the Supplementary Table 8). (d) The Paleo-climate evolution indicators modified after Wang et al. (2013). The results indicate a pronounced climate change between the Denglouku Fm. and Quantou Fm.. (e) AFT KDE of the Zhangguangcai Range and thermochronology age trends in the northeastern Songliao basin.

FIGURE 4

(a)–(b) 3D conceptual models of sedimentation and drainage evolution of the Shahezi, Yingcheng, Denglouku and Quantou Fms., modified after Cheng (2019); Feng et al. (2010); Wang et al. (2016), and sample locations are also indicated in Figure 2.

REFERENCE

An, D. Z. (2018). Early Cretaceous Sedimentary records and provenance analysis of the upper member of Shahezi formation in Songliao Basin. *Master's dissertation of China University of Geosciences* (in Chinese with English abstract).

Chen, H. H., Zhu, X. M., Gawthorpe, R. L., Wood, L. J., Liu, Q. H., Li, S. L., Shi, R. S., & Li, H. Y. (2022). The interactions of volcanism and clastic sedimentation in rift basins: Insights from the Palaeogene-Neogene Shaleitian uplift and surrounding sub-basins, Bohai Bay Basin, China. *Basin Research, 34,* 1084–1112. https://doi.org/10.1111/bre.12651.

Cheng, Y. H. (2019). Sedimentary filling and tectonic thermal events since Late Cretaceous in the Songliao Basin. *Doctoral Dissertation of China University of Geosciences* (in Chinese with

English abstract).

Elia, L., Martí, J., Muravchik, M., Bilmes, A., & Franzese, J. R. (2016). Impact of volcanism on the sedimentary record of the Neuquén rift basin, Argentina: towards a cause and effect model. *Basin Research, 30,* 311–335. https://doi.org/10.1111/bre.12222.

Feng, Z. Q., Jia, C. Z., Xie, X. N., Zhang, S., Feng, Z. H., & Cross, T. A. (2010). Tectonostratigraphic units and stratigraphic sequences of the nonmarine Songliao Basin, northeast China. *Basin Research, 22,* 79–95. https://doi.org/10.1111/j.1365-2117.2009.00445.x.

Friedmann, S. J., & Burbank, D. W. (1995). Rift basins and supradetachment basins: intracontinental extensional end-members. *Basin Research, 7,* 109–127. https://doi.org/10.1111/j.1365-2117.1995.tb00099.x.

Frostick, L. E., & Reid, I. (1989). Is structure the main control of river drainage and sedimentation in rifts? *Journal of African Earth Sciences (and the Middle East), 8,* 165–182. https://doi.org/10.1016/S0899-5362(89)80022-3.

Frostick, L. E., & Reid, I. (1990). Structural control of sedimentation patterns and implication for the economic potential of the East African Rift basins. *Journal of African Earth Sciences (and the Middle East), 10,* 307–318. https://doi.org/10.1016/0899-5362(90)90062-J.

Gawthorpe, R. L., & Leeder, M. R. (2000). Tectono-sedimentary evolution of active extensional basins. *Basin Research, 12,* 195–218. https://doi.org/10.1111/j.1365-2117.2000.00121.x.

Ge, R. F., Zhang, Q. L., Wang, L. S., Chen, J., Xie, G. A., & Wang, X. Y. (2012). Late Mesozoic rift evolution and crustal extension in the central Songliao Basin, northeastern China: constraints from cross-section restoration and implications for lithospheric thinning. *International*

Geology Review, 54, 183–207. https://doi.org/10.1080/00206814.2010.511900.

Goddard, A. S., & Carrapa, B. (2018). Effects of Miocene–Pliocene global climate changes on continental sedimentation: A case study from the southern Central Andes. *Geology, 46,* 647–650. https://doi.org/10.1130/G40280.1.

Jepson, G., Carrapa, B., Gillespie, J., Feng, R., DeCelles, P. G., Kapp, P., Tabor, C. R., & Zhu, J. (2021). Climate as the Great Equalizer of Continental-Scale Erosion. *Geophysical Research Letters, 48,* e2021GL095008. https://doi.org/10.1029/2021GL095008.

Khalil, S. M., & McClay, K. R. (2009). Structural control on syn-rift sedimentation, northwestern Red Sea margin, Egypt. *Marine and Petroleum Geology, 26,* 1018–1034. https://doi.org/10.1016/j.marpetgeo.2008.09.001.

Lambiase, J. J., & Bosworth, W. (1995). Structural controls on sedimentation in continental rifts. *Geological Society, London, Special Publications, 80,* 117–144. https://doi.org/10.1144/GSL.SP.1995.080.01.06.

Li, S. Q., Chen, F. K., Siebel, W., Wu, J. D., Zhu, X. Y., Shan, X. L., & Sun, X. M. (2012). Late Mesozoic tectonic evolution of the Songliao basin, NE China: Evidence from detrital zircon ages and Sr–Nd isotopes. *Gondwana Research, 22,* 943–955. https://doi.org/10.1016/j.gr.2012.04.002.

Li, S. Q., He, S., & Chen, F. K. (2020). Provenance changes across the mid-Cretaceous unconformity in basins of northeastern China: Evidence for an integrated paleolake system and tectonic transformation. *GSA Bulletin, 133,* 185–198. https://doi.org/10.1130/B35660.1.

Li, T., Yu, R. A., Wang, T. J., Yin, D. F., Si, Q. H., Zhu, Q., Wen, S. B., & Tu, J. R. (2021a). Geochemical characteristics, detrital zircon age and provenance analysis of Upper Cretaceous

Quantou Formation in Kalun Lake area, southeast margin of Songliao Basin. *Earth Science* (in Chinese with English abstract). https://doi:10.3799/dqkx.2021.264.

Li, Z. Q., Chen, J. L., Zou, H., Wang, C. S., Meng, Q. A., Liu, H. L., & Wang, S. Z. (2021b). Mesozoic–Cenozoic tectonic evolution and dynamics of the Songliao Basin, NE Asia: Implications for the closure of the Paleo-Asian Ocean and Mongol-Okhotsk Ocean and subduction of the Paleo-Pacific Ocean. *Earth-Science Reviews, 218,* 103471. https://doi.org/10.1016/j.earscirev.2020.103471.

Liu, H. B., Wang, P. J., Gao, Y. F., Hou, H. S., Yin, Y. K., Li, H. H., & Feng, Y. H. (2021). New data from ICDP borehole SK2 and its constraint on the beginning of the Lower Cretaceous Shahezi Formation in the Songliao Basin, NE China. *Science Bulletin, 66,* 411–413. https://doi.org/10.1016/j.scib.2020.12.002.

Liu, J. F., Chi, X. G., Dong, C. Y., Zhao, Z., Li, G. R., & Zhao, Y. D. (2008). Discovery of Early Paleozoic granites in the eastern Xiao Hinggan Mountains, northeastern China and their tectonic significance. *Geological Bulletin of China, 27,* 534–544 (in Chinese with English abstract).

Liu, K., Zhang, J. J., Xiao, W. J., Wilde, S. A., & Alexandrov, I. (2020a). A review of magmatism and deformation history along the NE Asian margin from ca. 95 to 30 Ma: transition from the Izanagi to Pacific plate subduction in the early Cenozoic. *Earth-Science Reviews, 209,* 103–317. https://doi.org/10.1016/j.earscirev.2020.103317.

Liu, S. (2020b). Demarcation of the boundary between Yingcheng Formation and Denglouku Formation of Lower Cretaceous in the north of Songliao Basin and paleoclimate change—Based on continuous coring data of SK2. *Master's Dissertation of Jilin University*

(in Chinese with English abstract).

Liu, Y. J., Li, W. M., Feng, Z. Q., Wen, Q. B., Neubauer, F., & Liang, C. Y. (2017). A review of the Paleozoic tectonics in the eastern part of Central Asian Orogenic Belt. *Gondwana Research, 43,* 123–148. https://doi.org/10.1016/j.gr.2016.03.013.

Ma, Q., & Xu, Y. G. (2021). Magmatic perspective on subduction of Paleo-Pacific plate and initiation of big mantle wedge in East Asia. *Earth-Science Reviews, 213,* 103473. https://doi.org/10.1016/j.earscirev.2020.103473.

Ma, X. J., Wu, H. C., Fang, Q., Shi, M. N., Zhang, S. H., Yang, T. S., Li, H. Y., & Wang, C. S. (2020). A floating astronomical time scale for the early Late Cretaceous continental strata in the Songliao Basin, northeastern China. *Acta Geologica Sinica, 94,* 27–37. https://doi.org/10.1111/1755-6724.14497.

Muravchik, M., Gawthorpe, R. L., Sharp, I. R., Rarity, F., & Hodgetts, D. (2018). Sedimentary environment evolution in a marine hanging wall dip slope setting. El Qaa Fault Block, Suez Rift, Egypt. *Basin Research, 30,* 452–478. https://doi.org/10.1111/bre.12231.

Olierook, H. K. H., Barham, M., Fitzsimons, I. C. W., Timms, N. E., Jiang, Q., Evans, N. J., & McDonald, B. J. (2019). Tectonic controls on sediment provenance evolution in rift basins: Detrital zircon U-Pb and Hf isotope analysis from the Perth Basin, Western Australia. *Gondwana Research, 66,* 126–142. https://doi.org/10.1016/j.gr.2018.11.002.

Pang, Y. M., Guo, X. W., Zhang, X. H., Zhu, X. Q., Hou, F. H., Wen, Z. H., & Han, Z. Z. (2020). Late Mesozoic and Cenozoic tectono-thermal history and geodynamic implications of the Great Xing'an Range, NE China. *Journal of Asian Earth Sciences, 189,* 104155. https://doi.org/10.1016/j.jseaes.2019.104155.

Song, Y., Ren, J. Y., Liu, K. Y., Lyu, D. W., Feng, X. J., Liu, Y., & Stepashko, A. (2022). Syn-rift to post-rift tectonic transition and drainage reorganization in continental rifting basins: Detrital zircon analysis from the Songliao Basin, NE China. *Geoscience Frontiers, 13,* 101377. https://doi.org/10.1016/j.gsf.2022.101377.

Suo, Y. H., Li, S. Z., Cao, X. Z., Wang, X. Y., Somerville, I., Wang, G. Z., Wang, P. C., & Liu, B. (2020). Mesozoic–Cenozoic basin inversion and geodynamics in East China: A review. *Earth-Science Reviews, 210,* 103357. https://doi.org/10.1016/j.earscirev.2020.103357.

Teixeira, B. M. N., Astini, R. A., Gomez, F. J., Morales, N., & Pimentel, M. M. (2018). Source-to-sink analysis of continental rift sedimentation: Triassic Cuyo basin, Precordillera Argentina. *Sedimentary Geology, 376,* 164–184. https://doi.org/10.1016/j.sedgeo.2018.08.007.

Tiercelin, J. J. (1990). Rift-basin sedimentation: responses to climate, tectonism and volcanism. Examples of the East African Rift. *Journal of African Earth Sciences (and the Middle East), 10,* 283–305. https://doi.org/10.1016/0899-5362(90)90061-I.

Wang, C. S., Feng, Z. Q., Zhang, L. M., Huang, Y. J., Cao, K., Wang, P. J., & Zhao, B. (2013). Cretaceous paleogeography and paleoclimate and the setting of SKI borehole sites in Songliao Basin, northeast China. *Palaeogeography, Palaeoclimatology, Palaeoecology, 385,* 17–30. https://doi.org/10.1016/j.palaeo.2012.01.030.

Wang, N., Zhang, Z. Y., Malusà, M. G., Wu, L., Chew, D., Zhang, J. E., Xiang, D. F., & Xiao, W. J. (2021). Pulsed Mesozoic exhumation in Northeast Asia: New constraints from zircon U-Pb and apatite U-Pb, fission track and (U-Th)/He analyses in the Zhangguangcai Range, NE China. *Tectonophysics, 818,* 229075. https://doi.org/10.1016/j.tecto.2021.229075.

Wang, N., Zhang, Z. Y., Malusà, M. G., Chew, D., Wu, L., Xiang, D. F., and Xiao, W. J. (2023). Late Mesozoic impact of paleo-Pacific subduction on the North China craton revealed by apatite U-Pb and fission-track double dating and trace element analysis in the eastern Yanshan fold belt, northeastern Asia. *GSA Bulletin*. https://doi.org/10.1130/B36751.1.

Wang, P. J., Chen, C. Y., & Liu, H. B. (2016a). Aptian giant explosive volcanic eruptions in the Songliao Basin and northeast Asia: A possible cause for global climate change and OAE-1a. *Cretaceous Research, 62,* 98–108. https://doi.org/10.1016/j.cretres.2015.09.021.

Wang, P. J., Mattern, F., Didenko, N. A., Zhu, D. F., Singer, B., & Sun, X. M. (2016b). Tectonics and cycle system of the Cretaceous Songliao Basin: an inverted active continental margin basin. *Earth-Science Reviews, 159,* 82–102. https://doi.org/10.1016/j.earscirev.2016.05.004.

Wang, S. Y., Cheng, Y. H., Jin, R. S., Miao, P. S., Zhang, T. F., Xu, Z. L., Ao, C., Teng, X. M., & Cheng, X. Y. (2022a). Detrital zircon U-Pb ages of the Cretaceous strata in the southern Songliao Basin, NE China: Constraints on basin-and-range evolution. *Sedimentary Geology, 433,* 106133. https://doi.org/10.1016/j.sedgeo.2022.106133.

Wang, T. T., Wang, C. S., Ramezani, J., Wan, X. Q., Yu, Z. Q., Gao, Y. F., He, H. Y., & Wu, H. C. (2022b). High-precision geochronology of the Early Cretaceous Yingcheng Formation and its stratigraphic implications for Songliao Basin, China. *Geoscience Frontiers, 13,* 101386. https://doi.org/10.1016/j.gsf.2022.101386.

Wu, F. Y., Sun, D. Y., Ge, W. C., Zhang, Y. B., Grant, M. L., Wilde, S. A., & Jahn, B. M. (2011). Geochronology of the Phanerozoic granitoids in northeastern China. *Journal of Asian Earth Sciences, 41,* 1–30. https://doi.org/10.1016/j.jseaes.2010.11.014.

Wu, G. L., Meng, Q. R., Zhu, R. X., Fan, L. G., Meng, K., Wei, H. H., Duan, L., & Zhu, J. C. (2021).

Middle Jurassic orogeny in the northern North China block. *Tectonophysics, 801,* 228713. https://doi.org/10.1016/j.tecto.2020.228713.

Xu, W. L., Pei, F. P., Wang, F., Meng, E., Ji, W. Q., Yang, D. B., & Wang, W. (2013). Spatial-temporal relationships of Mesozoic volcanic rocks in NE China: constraints on tectonic overprinting and transformations between multiple tectonic regimes. *Journal of Asian Earth Sciences, 74,* 167–193. https://doi.org/10.1016/j.jseaes.2013.04.003.

Yang, C. Z. (2014). Comparative study on Late Cretaceous tectonic inversion of Songliao Basin-Great Sanjiang Basin and its genetic relationships. *Doctoral Dissertation of China University of Geosciences* (in Chinese with English abstract).

Yang, X. B., Wang, H. Y., Li, Z. Y., Guan, C., & Wang, X. (2021). Tectonic-sedimentary evolution of a continental rift basin: A case study of the Early Cretaceous Changling and Lishu fault depressions, southern Songliao Basin, China. *Marine and Petroleum Geology, 128,* 105068. https://doi.org/10.1016/j.marpetgeo.2021.105068.

Yu, Z. Q., He, H. Y., Deng, C. L., Lu, K., Shen, Z. S., & Li, Q. L. (2020). New SIMS U-Pb geochronology for the Shahezi Formation from CCSD-SK-IIe borehole in the Songliao Basin, NE China. *Science Bulletin, 65,* 1049–1051. https://doi.org/10.1016/j.scib.2020.03.039.

Zhang, F. Q., Dilek, Y., Chen, H. L., Yang, S. F., & Meng, Q. A. (2017a). Late Cretaceous tectonic switch from a Western Pacific-to an Andean-Type continental margin evolution in East Asia, and a foreland basin development in NE China. *Terra Nova, 29,* 335–342. https://doi.org/10.1111/ter.12286.

Zhang, F. Q., Dilek, Y., Chen, H. L., Yang, S. F., & Meng, Q. A. (2017b). Structural architecture and stratigraphic record of Late Mesozoic sedimentary basins in NE China: tectonic archives of

the Late Cretaceous continental margin evolution in East Asia. *Earth-Science Reviews, 171,* 598–620. https://doi.org/10.1016/j.earscirev.2017.05.015.

Zhang, G. J. (2018). Age constraints on thermochronometry of Dongling-Lishu fault within Songliao Basin. *Master dissertation of Jilin University* (in Chinese with English abstract).

Zhang, J. H., Gao, S., Ge, W. C., Wu, F. Y., Yang, J. H., Wilde, S. A., & Li, M. (2010). Geochronology of the Mesozoic volcanic rocks in the Great Xing'an Range, northeastern China: implications for subduction-induced delamination. *Chemical Geology, 276,* 144–165. https://doi.org/10.1016/j.chemgeo.2010.05.013.

Zhang, J., Liu, Y. G., Flögel, S., Zhang, T., Wang, C. S., & Fang, X. M. (2021). Altitude of the East Asian Coastal Mountains and Their Influence on Asian Climate During Early Late Cretaceous. *Journal of Geophysical Research: Atmospheres, 126,* e2020JD034413. https://doi.org/10.1029/2020JD034413.

Zhang, L. M., Wang, C. S., Cao, K., Wang, Q., Tan, J., & Gao, Y. (2016). High elevation of Jiaolai Basin during the Late Cretaceous: Implication for the coastal mountains along the East Asian margin. *Earth and Planetary Science Letters, 456,* 112–123. https://doi.org/10.1016/j.epsl.2016.09.034.

Zhang, S. H., Zhao, Y., Davis, G. A., Ye, H., & Wu, F. (2014). Temporal and spatial variations of Mesozoic magmatism and deformation in the North China Craton: Implications for lithospheric thinning and decratonization. *Earth-Science Reviews, 131,* 49–87. https://doi.org/10.1016/j.earscirev.2013.12.004.

Zhao, B., Wang, C. S., Wang, X. F., & Feng, Z. Q. (2013). Late Cretaceous (Campanian) provenance change in the Songliao Basin, NE China: evidence from detrital zircon U-Pb ages from the

Yaojia and Nenjiang Formations. *Palaeogeography, Palaeoclimatology, Palaeoecology, 385,* 83–94. https://doi.org/10.1016/j.palaeo.2012.03.017.

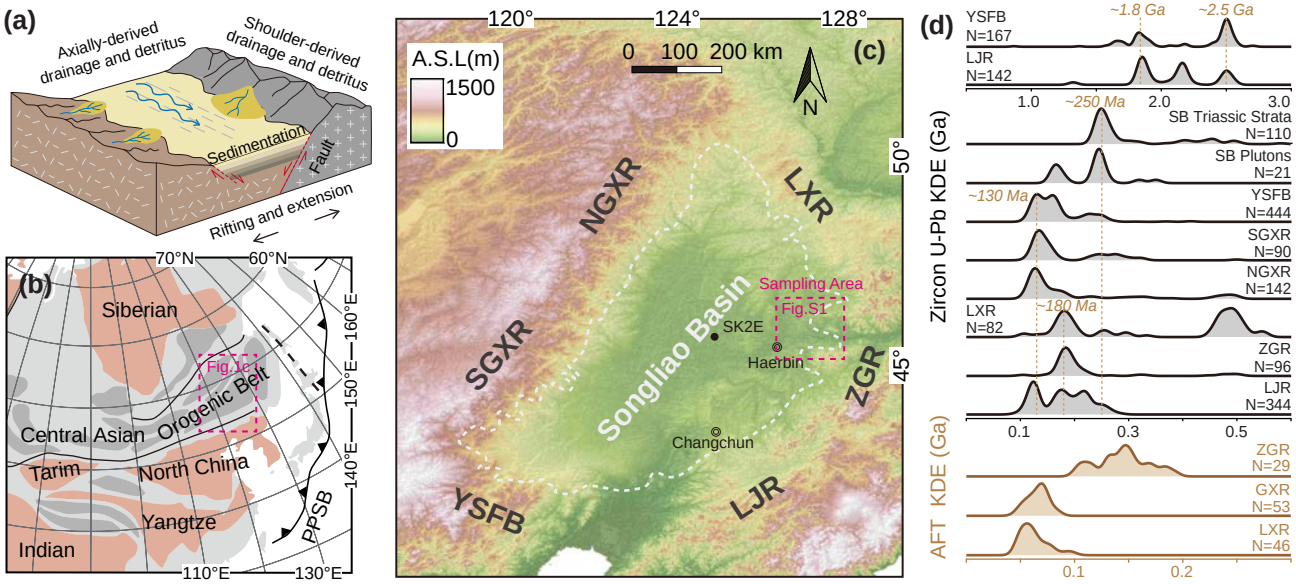
(a)
Axially-derived drainage and detritus
Shoulder-derived drainage and detritus
Sedimentation
Fault
Rifting and extension
(b)
70°N
60°N
160°E
150°E
140°E
110°E
130°E
Siberian
Fig.1c
Central Asian Orogenic Belt
Tarim
North China
Yangtze
Indian
PPSB
(c)
120°
124°
128°
50°
45°
A.S.L(m)
1500
0
0 100 200 km
N
NGXR
LXR
SGXR
ZGR
YSFB
LJR
Songliao Basin
Sampling Area
Fig.S1
SK2E
Haerbin
Changchun
(d)
Zircon U-Pb KDE (Ga)
~1.8 Ga
~2.5 Ga
~250 Ma
~130 Ma
~180 Ma
YSFB N=167
LJR N=142
SB Triassic Strata N=110
SB Plutons N=21
YSFB N=444
SGXR N=90
NGXR N=142
LXR N=82
ZGR N=96
LJR N=344
1.0
2.0
3.0
0.1
0.3
0.5
AFT KDE (Ga)
ZGR N=29
GXR N=53
LXR N=46
0.1
0.2

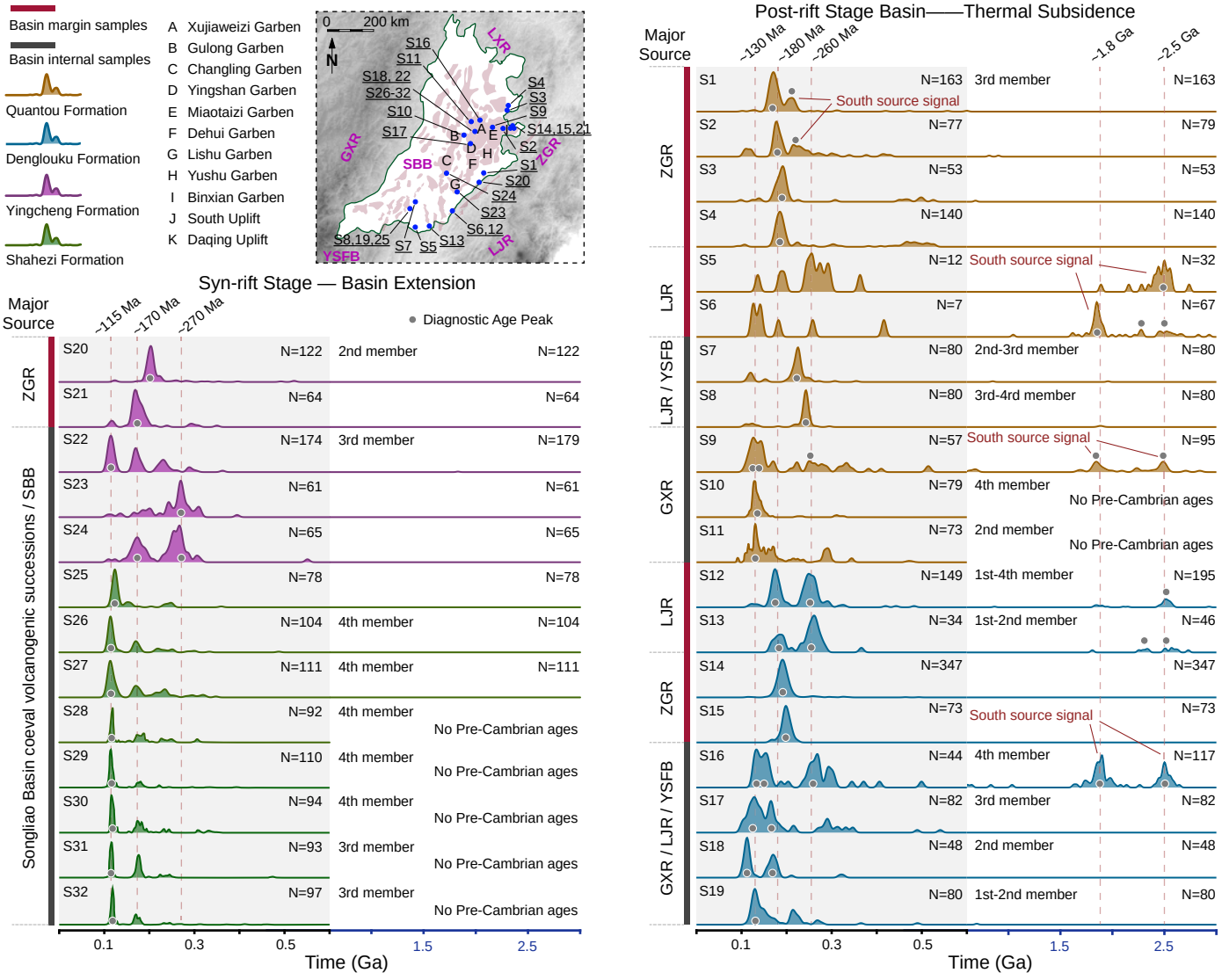
Basin margin samples
Basin internal samples
Quantou Formation
Denglouku Formation
Yingcheng Formation
Shahezi Formation
A Xujiaweizi Garben
B Gulong Garben
C Changling Garben
D Yingshan Garben
E Miaotaizi Garben
F Dehui Garben
G Lishu Garben
H Yushu Garben
I Binxian Garben
J South Uplift
K Daqing Uplift
0 200 km
N
S16
S11
S18, 22
S26-32
S10
S17
S4
S3
S9
S14,15,21
S2
S1
S20
S24
S23
S6,12
S13
S5
S7
S8,19,25
LXR
GXR
SBB
ZGR
LJR
YSFB
Syn-rift Stage — Basin Extension
Major Source
~115 Ma
~170 Ma
~270 Ma
Diagnostic Age Peak
ZGR
Songliao Basin coeval volcanogenic successions / SBB
S20 N=122 2nd member N=122
S21 N=64 N=64
S22 N=174 3rd member N=179
S23 N=61 N=61
S24 N=65 N=65
S25 N=78 N=78
S26 N=104 4th member N=104
S27 N=111 4th member N=111
S28 N=92 4th member No Pre-Cambrian ages
S29 N=110 4th member No Pre-Cambrian ages
S30 N=94 4th member No Pre-Cambrian ages
S31 N=93 3rd member No Pre-Cambrian ages
S32 N=97 3rd member No Pre-Cambrian ages
0.1
0.3
0.5
1.5
2.5
Time (Ga)
Post-rift Stage Basin——Thermal Subsidence
Major Source
~130 Ma
~180 Ma
~260 Ma
~1.8 Ga
~2.5 Ga
ZGR
LJR
LJR / YSFB
GXR
LJR
ZGR
GXR / LJR / YSFB
S1 N=163 3rd member N=163
South source signal
S2 N=77 N=79
S3 N=53 N=53
S4 N=140 N=140
S5 N=12 South source signal N=32
S6 N=7 N=67
S7 N=80 2nd-3rd member N=80
S8 N=80 3rd-4rd member N=80
S9 N=57 South source signal N=95
S10 N=79 4th member No Pre-Cambrian ages
S11 N=73 2nd member No Pre-Cambrian ages
S12 N=149 1st-4th member N=195
S13 N=34 1st-2nd member N=46
S14 N=347 N=347
S15 N=73 South source signal N=73
S16 N=44 4th member N=117
S17 N=82 3rd member N=82
S18 N=48 2nd member N=48
S19 N=80 1st-2nd member N=80
0.1
0.3
0.5
1.5
2.5
Time (Ga)

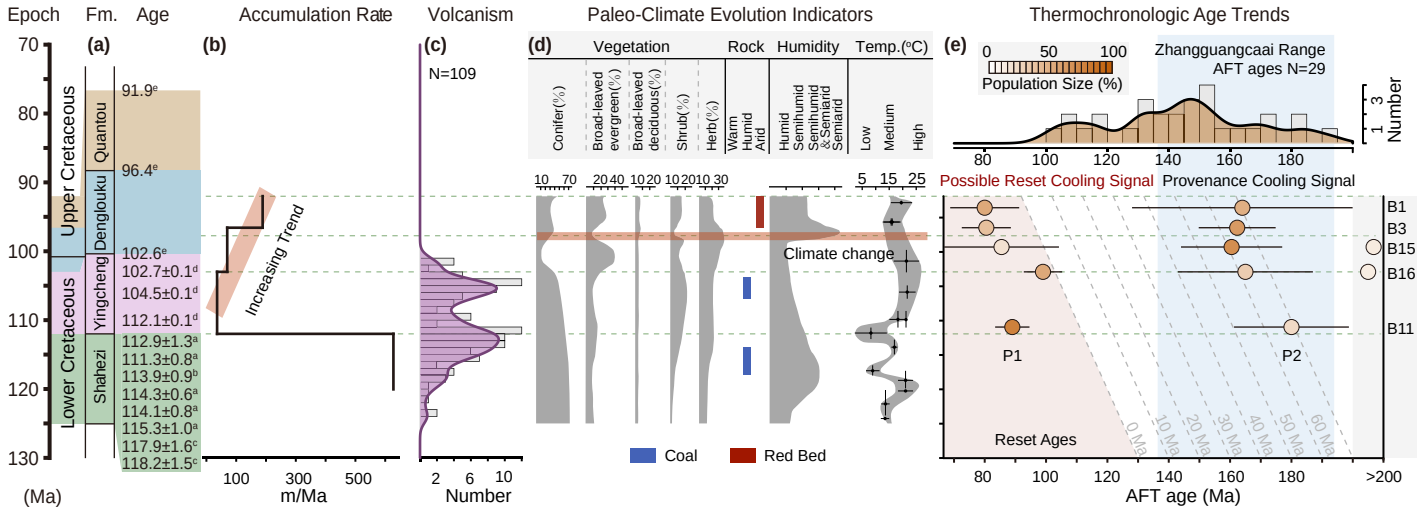
Epoch
Fm.
Age
Accumulation Rate
Volcanism
Paleo-Climate Evolution Indicators
Thermochronologic Age Trends
(a)
(b)
(c)
(d)
(e)
Upper Cretaceous
Lower Cretaceous
Quantou
Denglouku
Yingcheng
Shahezi
91.9e
96.4e
102.6e
102.7±0.1d
104.5±0.1d
112.1±0.1d
112.9±1.3a
111.3±0.8a
113.9±0.9b
114.3±0.6a
114.1±0.8a
115.3±1.0a
117.9±1.6c
118.2±1.5c
70
80
90
100
110
120
130
(Ma)
Increasing Trend
100
300
500
m/Ma
N=109
2
6
10
Number
Vegetation
Rock
Humidity
Temp.(°C)
Conifer(%)
Broad-leaved evergreen(%)
Broad-leaved deciduous(%)
Shrub(%)
Herb(%)
Warm
Humid
Arid
Humid
Semihumid
Semihumid &Semiarid
Semiarid
Low
Medium
High
10 70
20 40
10 20
10 20
10 30
5 15 25
Climate change
Coal
Red Bed
0
50
100
Population Size (%)
Zhangguangcaai Range
AFT ages N=29
1
3
Number
80
100
120
140
160
180
Possible Reset Cooling Signal
Provenance Cooling Signal
B1
B3
B15
B16
B11
P1
P2
Reset Ages
0 Ma
10 Ma
20 Ma
30 Ma
40 Ma
50 Ma
60 Ma
>200
AFT age (Ma)

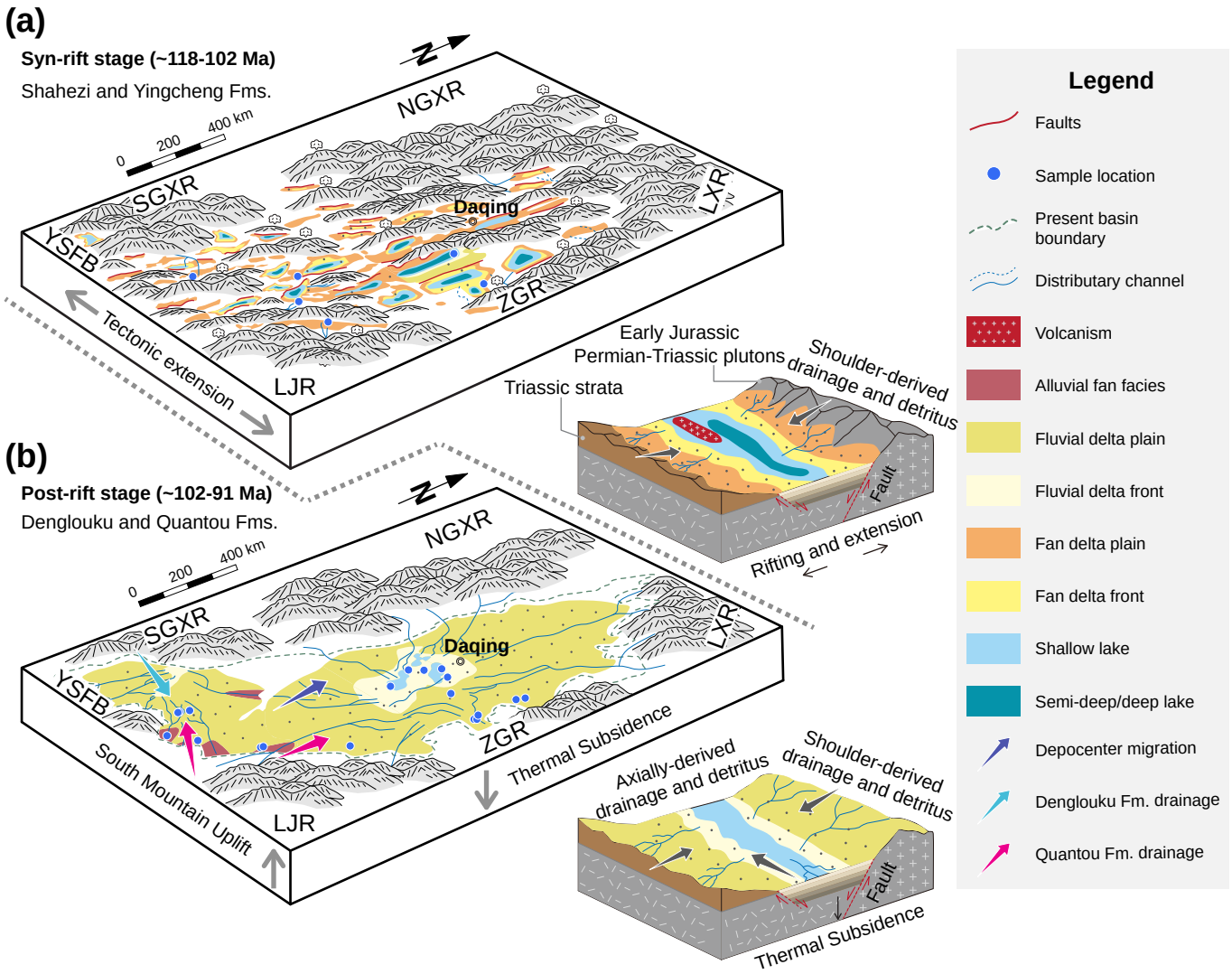
(a)
Syn-rift stage (~118-102 Ma)
Shahezi and Yingcheng Fms.
N
0
200
400 km
NGXR
SGXR
LXR
YSFB
Daqing
ZGR
LJR
Tectonic extension
Early Jurassic
Permian-Triassic plutons
Triassic strata
Shoulder-derived
drainage and detritus
Fault
Rifting and extension
(b)
Post-rift stage (~102-91 Ma)
Denglouku and Quantou Fms.
N
0
200
400 km
NGXR
SGXR
LXR
YSFB
Daqing
ZGR
LJR
South Mountain Uplift
Thermal Subsidence
Axially-derived
drainage and detritus
Shoulder-derived
drainage and detritus
Fault
Thermal Subsidence
Legend
Faults
Sample location
Present basin boundary
Distributary channel
Volcanism
Alluvial fan facies
Fluvial delta plain
Fluvial delta front
Fan delta plain
Fan delta front
Shallow lake
Semi-deep/deep lake
Depocenter migration
Denglouku Fm. drainage
Quantou Fm. drainage

Supporting Information

Geo-thermochronological analysis reveals transition from transverse to axial detrital inputs during Cretaceous rifting in the Songliao Basin, NE China

Nan Wang[a,b,c], Zhiyong Zhang[a]*, Marco G. Malusà[c]*, Jien Zhang[a], Lin Wu[a], Dunfeng Xiang[a,b], Wenjiao Xiao[d]

[a]State Key Laboratory of Lithospheric Evolution, Institute of Geology and Geophysics, Chinese Academy of Sciences, Beijing 100029, China

[b]University of Chinese Academy of Sciences, Beijing 100049, China

[c]Department of Earth and Environmental Sciences, University of Milano-Bicocca, Milano 20126, Italy

[d]Xinjiang Research Center for Mineral Resources, Xinjiang Institute of Ecology and Geography, Chinese Academy of Sciences, Urumqi 830011, China

……..

Contents

Figure S1 Geological sketch map and stratigraphic column of northeastern Songliao basin.

Figure S2 Vertical basin fill sequence of the Songliao basin.

Figure S3 Outcrop photographs showing the main observed lithologies and facies of the sedimentary rocks in the northeastern Songliao basin.

Figure S4 Microscopy photographs (taken under crossed polarizers) displaying petrographic features of sedimentary rocks samples in the northeastern Songliao basin.

Figure S5 Representative cathodoluminescence (CL) images of zircons from sedimentary rocks in the northeastern Songliao basin.

Figure S6 Cumulative zircon U-Pb age distributions and KDE for the samples in the northeastern Songliao basin.

Figure S7 U-Pb concordia diagrams of sedimentary samples collected from the northeastern Songliao basin.

Figure S8 U-Pb concordia diagrams of volcanic rock samples collected from the northeastern Songliao basin.

Figure S9 AFT radial plots and support vector machine (SVM) apatite categorization scheme for the sedimentary rock and volcanic samples of the northeastern Songliao basin.

Figure S10 The classic multidimensional scaling plot for zircon U-Pb ages of the Songliao Basin and surrounding potential provenance.

Figure S11 Cretaceous stratigraphy column and depositional facies map of the Binxian depression, northeastern Songliao basin.

Figure S12 Depositional facies map of the Yingcheng and Shahezi Formations in the Shuangliao, Lishu and Xujiaweizi Grabens, northeastern Songliao basin.

Figure S13 Grabens distribution and tectonic evolution of A-A’ seismic reflection profiles in northeastern Songliao basin.

Figure S14 Regional seismic interpreted profile across the northern part of the Songliao Basin.

Figure S15 Key period 4D reconstruction of mid-Cretaceous tectonic evolution in the northeastern Songliao Basin.

Figure S16 ZHe age-elevation relationships from Dahaituo plutons of the eastmost YSFB and Fenghuangshan and Xiemashan granites of the LJR, and cooling curves of several plutons from the

north NCC.

Table S1 Summarized characteristics of samples from the northeastern Songliao basin, northeast China.

Table S2 Apatite FT data of sedimentary and volcanic rocks samples from the northeastern Songliao basin, northeast China.

Table S3 Summarized information of previous published detrital zircon U-Pb and Hf isotopic samples from the Songliao Basin, northeast China.

Table S4 Summary of axial direction, sedimentary facies and major faults of major grabens from the Songliao Basin, northeast China.

Supplementary Table 1 Data of single-grain zircon U-Pb dating.

Supplementary Table 2 Data of single-grain apatite fission track analysis.

Supplementary Table 3 Data of single-grain apatite trace element.

Supplementary Table 4 Summarized magmatism crystallization ages from the potential provenance surrounding the Songliao Basin.

Supplementary Table 5 Summarized apatite fission track ages data of the basement of the Great Xing'an Range, Zhangguangcai Range and Lesser Xing'an Range.

Supplementary Table 6 Summarized detrital zircon U-Pb ages data of the Shahezi, Yingcheng, Denglouku and Quantou Formations.

Supplementary Table 7 Zircon U-Pb ages of the Songliao Basin basement (including plutons and strata).

Supplementary Table 8 Zircon U-Pb and Ar-Ar ages of the late Early Cretaceous volcanic rocks in and around the Songliao Basin.

1. Sample description

The study area, also known as Binxian depression, is located at the northeastern margin of the Songliao Basin (Figure 1c), where late Early Cretaceous sedimentary successions are sporadically outcropped in several regions (Figure S1). Eighteen samples, including sixteen sandstone and two volcanics samples, were collected for this study (Figure S1; Table S1).

Samples B1 and B2 were collected from the outcrop at the Yonggan village of Qingan county (Figure S1), which changes up from brown coarse sandstone with interbedded grayish mudstone and gravels, to the brown conglomerate and pebbly sandstone couplets (Figures S2, S3, and S4). It indicates a fluvial delta plain facies environment. Samples B1 and B2 were taken from the brown coarse sandstone and conglomerate layers respectively, with an occurrence of 62°∠9° (Figures S2, S3, and S4).

The outcrop for sample B3 was exposed at the Sujia village, Bin county (Figure S1), and is dominated by brown coarse thick sandstone and conglomerate couplets (Figures S2, S3, and S4). Sample B3 was taken from the coarse sandstone layer (Figures S2, S3, and S4).

Samples B4, B5, B6, B7, and B8 were taken from a small section outcropped at the Hengtai village of Qingan county (Figure S1). This section ranges upwards from thick grayish greywacke with interbedded thin amaranth mudstone, through thin gray tuff layer, to grayish tuffaceous greywacke and amaranth mudstone couplets (Figures S2, S3, and S4) and represents the fluvial facies. This section has an occurrence of 353°∠9° at the lower part and 345°∠9° at the upper part, respectively (Figure S3). Samples B7 and B8 were collected from the greywacke layers at the bottom (Figures S2, S3, and S4), whereas samples B4, B5, and B6 are the tuffaceous greywacke or tuff at the top (Figures S2, S3, and S4). Abundant volcanic quartz grains and a small number of lithic grains were observed in samples B4, B7, and B8 (Figure S4).

A series of volcanic-sedimentary strata were exposed at the Mengjia village of Bin county (Figure S1), which is composed mainly of the dark-red basalt andesite, yellow-green basalt andesite, and dark-red andesitic crystal tuff, with the occurrence of 271°∠29° (Figures S2, S3, and S4). Samples B9, B10, and B11 were sampled from the dark-red basalt andesite, yellow-green basalt andesite, and dark-red andesitic crystal tuff layers, respectively (Figures S2, S3, and S4).

Another outcrop, ~2.5 km east of the previous sampling location (B9, B10 and B11), is located at the Moshigang village of Bin county (Figure S1). This small outcrop varies from alternating of thick

brown greywacke and thin grayish tuffaceous siltstone, to thick brown tuffaceous sandstone (Figures S2, S3, and S4). The general occurrence of the sedimentary rocks is about 191°∠10°. Samples B15, B14, B13, and B12 were taken from greywacke, tuffaceous siltstone, greywacke, and tuffaceous sandstone layers of this outcrop, respectively (Figures S2, S3, and S4). Volcanic quartz grains were observed from the tuffaceous sandstone, whereas greywacke contains few volcanic grains (Figure S4).

Sample B16 was collected from the sandstone outcrop situated at ~15 km northeast of the previous sample location (Figure S1). It mainly consists of alternating of brown coarse sandstone and fine sandstone with the occurrence of 356°∠46°, and sample B16 is the medium sandstone from this outcrop (Figures S2, S3, and S4).

Samples B17 and B18 are the amaranth welded tuff and grey welded tuff exposed at ~1 km north of the Yongcai village of Bin county (Figure S1).

2. Methodology

2.1 Zircon U-Pb dating analysis

Zircon U-Pb analyses for the Batch 1 and 3 were analyzed at the Beijing Quick-Thermo Science & Technology Co., Ltd, using an ESI New Wave NWR 193^{UC} (TwoVol2) laser ablation system connected to an Agilent 8900 ICP-QQQ, following analytical procedures described in Ji et al. (2020). Data reduction was conducted off-line using Iolite package which runs within the Igor Pro program (Paton, Hellstrom, Paul, Woodhead, & Hergt, 2011). Batch 2 were performed on an Agilent 7500a quadrupole ICP-MS equipped with a 193 nm Excimer ArF laser ablation system at the Beijing Createch Testing Technology Co., Ltd. Data reduction was conducted off-line by ICPMSDataCal program (Y. Liu et al., 2009). Zircon 91500 (Wiedenbeck et al., 1995) was used as primary reference material for all U-Pb age determinations. The weighted mean U-Pb ages and concordia plots were processed using Isoplot 4.15. Adaptive kernel density estimate and corresponding histograms were processed by the Isoplot R (Vermeesch, 2018). For these zircons with the U-Pb ages younger than 1500 Ma, the $^{206}Pb/^{238}U$ ages were used, whereas the $^{207}Pb/^{206}Pb$ ages were used for these zircons older than 1500 Ma, according to (Spencer, Kirkland, & Taylor, 2016).

2.2 Apatite fission track (FT) and trace element (TE) compositions analyses

Apatite FT analysis was performed at the Institute of Geology and Geophysics, Chinese Academy of Sciences (IGGCAS). Polished mounts embedded with apatite grains were etched in 5M nitric acid at 20°C for 20 seconds to reveal the spontaneous fission tracks. Gold coating (~5–7 nm thickness) was

applied to the etched mounts within a vacuum chamber in order to strengthen the reflectivity of the polished surface and minimize internal reflections under the microscope (Gleadow et al., 2009). Apatite crystals with polished surfaces parallel to prismatic crystal faces and homogeneous track distributions were selected and imaged using a Zeiss Axio Imager M2m Autoscan System. The TrackWorks software was used to capture stacks of high-resolution digital images with a ×100 dry objective under both transmitted and reflected light using a highly-sensitive and fast iDS camera. The dimensions of the images were precisely calibrated using a graticule. Manual counting of fission tracks was carried out using the accompanying FastTracks software using the coincidence mapping technique (Gleadow et al., 2009). FastTracks was also used to manually measure true confined track lengths, track etch pit diameters parallel to the crystallographic c-axis (D_{par}) and their orientation with respect to the crystallographic c-axis direction.

The *in situ* quantification of ^{238}U concentrations and trace elements for each counted grain was measured simultaneously from the same sampled aliquots through 30 μm spot analyses using an Agilent 8900 ICP-QQQ coupled with an ESI New Wave NWR 193^{UC} (TwoVol2) laser ablation system, at the Beijing Quick-Thermo Science & Technology Co., Ltd. Ablation was carried out over 20 seconds on the selected grains and reference materials (primary NIST SRM 612 glass and secondary apatite Mud Tank) with a 30 μm diameter beam size, ~3.0 J/cm^2 energy and 5 Hz repetition rate. Background subtraction and correction for laser downhole elemental fractionation for the time-resolved LA-ICPMS data were performed using the Iolite data reduction package within the Wavemetrics Igor Pro data analysis software (Paton et al., 2011). Single grain AFT ages were calculated using an absolute calibration based on primary constants (aggregate $\xi = 2.001\times10^{-3}$). Isoplot R (Vermeesch, 2018) was used to prepare radial plots and illustrate the distribution of individual grain ages together with the corresponding D_{par} values, and to deconvolve grain-age distributions into statistically meaningful grain-age populations. The detailed analytical procedures were described in Guo et al. (2022), N. Wang et al. (2021), Zhang et al. (2023).

3. Results

3.1 Zircon U-Pb dating results

628 zircon grains from eight samples collected from the Quantou Formation (B1, B3, B4, and B8), Denglouku Formation (B12, B15, and B16), and Yingcheng Formation (B11) were performed for zircon U-Pb dating analysis. Except for 78 grains with discordance ages (discordance > 10%), the

remaining 550 zircon grains are adequate for the evaluation of provenance. Also in the case, two volcanic rock samples were also analyzed by the zircon U-Pb dating technique. All zircon U-Pb data obtained in this study are listed in the Supplementary Table 1. Cumulative age distribution, adaptive kernel density estimation plots and corresponding histograms, as well as pie charts are exhibited in Figure S6. Representative cathodoluminesce (CL) images and concordia diagrams are shown in Figures S5 and S7.

The detrital zircon U-Pb data of the eight samples show the age range from 99 to 904 Ma (Figures S6 and S7; Table S1), and most of the zircons record the Late Triassic–Middle Jurassic ages and fall in the 220–160 Ma age range with primary age peak at 200–165 Ma (Figures S6 and S7; Table S1). Some early Paleozoic zircons exist in samples B1, B4 and B8 of the Quantou Formation, which could be framed into subordinate groups of 430–409 and 528–446 Ma (Figures S6 and S7; Table S1). Besides, sample B3 also show a relatively large proportion of the Late Paleozoic–Early Mesozoic ages, peaking at ~228 Ma and ~266 Ma (Figures S6 and S7; Table S1). Most zircons from these samples are subhedral to euhedral in shape and show oscillatory zoning in CL images (Figure S5), suggesting a predominantly detrital input from magmatic origin.

Detrital zircons from sample B1 are mostly subhedral to euhedral and variable in size with length/width ratios of ~1:1–1:3. In CL images, most of zircons show banded internal structures, suggesting a predominantly detrital input from magmatic origin (Figure S5). 54 usable ages were obtained from the 74 analyzed zircons. Zircon U-Pb ages range from 99 to 684 Ma, with two main peaks at ~179 Ma and ~195 Ma, and one minor peak at ~495 Ma (Figures S6 and S7; Table S1). A youngest age of 98.5 ± 2.9 Ma could define a limit on the maximum depositional age of this sample (Figures S6 and S7; Table S1), indicating the sample collected from the Quantou Formation.

Samples B8 and B4 were collected from a small sedimentary section of Quantou Formation (Figure S1), and yielded the similar age spectrums of detrital zircons (Figures S6 and S7). These zircons from sample B8 are mostly uniform in grain-size, euhedral in shape, with length/width ratios of 1:1–1:3. Most of them show oscillatory zoning in CL images and Th/U ratios for these grains range from 0.23 to 2.09, indicating a predominant detrital input from magmatic rocks (Figure S5). 71 usable zircon U-Pb analyses were obtained from 78 analyses, and yielded four age groups of 199–168 Ma, 226–215 Ma, 311–293 Ma and 527–428 Ma, with peaks at ~175 Ma, ~187 Ma, ~220 Ma, ~301 Ma, ~461 Ma, ~496 Ma, and ~518 Ma, respectively (Figures S6 and S7; Table S1). Similar with sample

B8, zircons from sample B4 are euhedral and uniform in size, with an average length of ~100 μm (Figure S5). The banded internal structures also can be recognized from their CL images (Figure S5), indicating a magmatic origin. The Th/U ratios of these zircons also show high values and vary from 0.26 to 1.21, except for one analysis with a low value of 0.09. 69 concordant and near concordant ages from 79 analyses show an age range from 528 to 104 Ma, and form a principal group at 202–171 Ma, with major peaks at ~175 and ~187 Ma, and three subordinate groups of 109–104 Ma, 260–225 Ma and 528–458 Ma (Figures S6 and S7; Table S1). The three youngest grains give a weighted mean age limiting the maximum depositional age of two samples from the Quantou Formation to 107.5 ± 3.0 Ma (Figures S6 and S7; Table S1).

These zircons from sample B3 show some variations in size and the largest grains have a length of ~200 μm, but most of these grains range between 50 and 100 μm in length. Some small zircon grains are rounded in shape, perhaps implying a longer transport distance from their source. However, most grains express euhedral or subhedral forms and oscillatory zoning in CL images, indicating a dominantly magmatic origin (Figure S5). In Figure S6, detrital zircons preserve a more restricted range of old U-Pb ages. Out of 91 grains analyzed, 79 zircon ages are usable and range widely from 904 to 107 Ma, which have four primary peaks at ~176 Ma, ~191 Ma, ~218 Ma, ~244 Ma, and several secondary age peaks at ~107 Ma, ~120 Ma, ~266 Ma and ~426 Ma (Figures S6 and S7; Table S1). Maximum depositional age for this sandstone sample is defined by the weighted mean age of the three youngest zircon grains at 107.1 ± 4.4 Ma (Figures S6 and S7; Table S1), implying the sample from the Quantou Formation.

Samples B15 and B12 were collected from the lower greywacke and upper tuffaceous sandstone layers of the same outcrop, respectively (Figure S1). Zircons from sample B15 are mostly subhedral to euhedral and almost all display oscillatory zoning (Figure S5). These zircons are mostly uniform in grain-size with length/width ratios of 1:1–1:2. Among the 67 usable ages from 73 analyses, almost all zircons are Late Triassic–Middle Jurassic ranging from 216 to 176 Ma except for several Paleozoic ages, with the main peaks at ~182 Ma, ~191 Ma and ~208 Ma (Figures S6 and S7; Table S1). However, these zircons from sample B12 show somewhat variations in size, some crystals have a length of ~200–100 μm, but most of these crystals are <100 μm in length. These grains mostly are subhedral to euhedral in shape and show distinct oscillatory growth zoning under CL images (Figure S5). Out of 84 grains analyzed, 73 zircon ages are usable and show a wide range from 493 to 112 Ma (Figure S6; Table S1).

There are abundant zircons forming an age cluster between 211 and 165 Ma, with major peaks at ~176 Ma, ~194 Ma and ~208 Ma (Figures S6 and S7; Table S1). The two youngest zircons show a weighted mean $^{206}Pb/^{238}U$ age of 115.4 ± 2.7 Ma and provide a limit on the maximum depositional age (Figures S6 and S7; Table S1), indicating the two samples collected from the Denglouku Formation.

Sample B11 shows somewhat variation in detrital zircon age pattern (Figures S6 and S7; Table S1). These zircons are mostly uniform in grain-size and most of these are euhedral in grain-shape, characterized by banded internal structures (Figure S5). The majority of Th/U ratios vary from 0.22 to 1.79, implying a dominant majority of magmatic zircons. 68 U-Pb analysis spots were obtained from 68 zircon crystals, 64 of which are concordant (Figures S6 and S7; Table S1). These ages show a range from 350 to 112 Ma, and cluster around 120–112 Ma, 198–161 Ma and 309–289 Ma, with the main peaks at ~167 Ma, ~178 Ma, and the minor peaks at ~118 Ma, ~195 Ma and ~301 Ma, respectively (Figures S6 and S7; Table S1). The five youngest zircon grains show a weighted mean $^{206}Pb/^{238}U$ age of 117.6 ± 4.5 Ma, which could be used to limit the deposition age, corresponding to the Yingcheng Formation.

For the sample B16, 73 usable zircon U-Pb ages were obtained from 81 analyses and preserve a less restricted range of detrital zircon ages. These zircons are variable in size, subhedral to euhedral in shape and most zircons show oscillatory zoning (Figure S5). All concordant analyses record the Late Triassic–Middle Jurassic ages and cluster around 224–166 Ma, with the main peaks at ~181 Ma, ~200 Ma, ~213 Ma, and minor peaks at ~167 Ma and ~223 Ma (Figures S6 and S7; Table S1).

Two volcanic rock samples (B17, B18) are the welded tuff and yielded the weighted mean $^{206}Pb/^{238}U$ age of 179 ± 1 Ma (n = 26, MSWD = 0.69, Figure S8) with Th/U ratios ranging from 0.46 to 1.13, and the weighted mean $^{206}Pb/^{238}U$ age of 182 ± 2 Ma (n = 21, MSWD = 1.4, Figure S8) with Th/U ratio ranging from 0.47 to 0.98, respectively. These results support an Early Jurassic eruption age for the volcanics of the Ningyuancun Formation.

3.2 Apatite fission track (FT) and trace element compositions results

The summarized AFT data and radial plots for the analyzed samples are shown in Table S2 and Figure 9, respectively. Trace element chemistry of detrital apatite grains is a useful approach to extract host rock-type information (G. O'Sullivan, Chew, Kenny, Henrichs, & Mulligan, 2020). To attain this, trace element compositions information for every unknown detrital apatite is required to be plotted on Sr/Y versus ΣLREE (La, Ce, Pr, Nd) discriminant biplots (G. O'Sullivan et al., 2020), which is

superposed on the large bedrock reference dataset (G. O'Sullivan et al., 2020; G. J. O'Sullivan, Chew, Morton, Mark, & Henrichs, 2018), categorized by the machine-learning algorithm (support vector machine, SVM). Low-or high-grade metamorphic rocks, or several sub-categories of igneous rocks origin for the apatite unknowns could be determined from the biplot. The support vector machine (SVM) apatite classification diagrams are also displayed in Figure 9. The detailed apatite fission track and trace element data from the analyzed apatite unknowns are available in the Supplementary Tables 2 and 3.

3.2.1 Yingcheng Formation

Sample B11 from the andesitic crystal tuff layer of Yingcheng Formation (~125–105 Ma; P. Wang et al., 2016), whose maximum depositional age is constrained at ~118 Ma by the youngest zircon U-Pb age group (Figure S6; Table S1), yielded two AFT age populations at ~89 Ma (77% data) and ~179 Ma (23% data) (Figure S9; Table S2). The dominant younger AFT age population is younger than its depositional age, indicative of significant residence in the AFT partial annealing zone (PAZ) after the deposition. It is also evidenced by the broad confined track lengths distribution with a MTL of 12.6 ± 1.6 μm (Figure S9; Table S2).

3.2.2 Denglouku Formation

Sample B16 was collected from the sandstone layer of lower member of Denglouku Formation (~103–96 Ma, Figure 3), whose 82 individual AFT ages can be separated into three populations of ~99 Ma (55% data), ~165 Ma (33% data), and ~334 Ma (12% data) (Figure S9; Table S2). The youngest AFT population is younger than its depositional age estimated at less than 118 Ma (Figure S6), indicating significant residence in the AFT PAZ after the deposition. The confined track lengths distribution shows a MTL of 12.7 ± 2.0 μm (Table S2).

Sample B15 was collected from the greywacke layer of Denglouku Formation (~103–96 Ma, Figure 3), and its depositional age can be constrained at ~115 Ma by the youngest zircon U-Pb age group from the above tuffaceous sandstone layer (Figure S6; Table S1). An Early Cretaceous age population of ~85 Ma (P1, 17% data), a Middle Jurassic age population of ~161 Ma (P2, 70% data) and a Carboniferous age population of ~313 Ma (P3, 13% data) are distinguished from these 65 AFT single-grain ages (Figure S9; Table S2). The Early Cretaceous AFT age population of ~85 Ma is also younger than its estimated depositional age, possibly indicating significant residence within the AFT PAZ after the deposition.

3.2.3 Quantou Formation

Sample B3 was deposited at ~100–94 Ma, whose 67 analyzed apatite crystals can be clearly separated into two AFT populations of ~81 Ma (P1, 38 %) and ~162 Ma (P2, 62 %), with a MTL distribution of 12.7 ± 2.0 μm (Figure S9; Table S2). The existence of younger AFT population that is younger than its depositional age indicates significant residence within the AFT PAZ after the deposition. Most of these apatite grains were plotted in the 'I+M' field, whereas some apatite crystals lying in the 'LM' and 'HM' field are also detected (Figure S9).

For sample B1, 13 individual AFT ages range from 198 Ma to 64 Ma and can be statistically decomposed into two age populations: a Late Cretaceous age of 79.9 ± 11.3 Ma (P1, 51 % data) and a Middle Jurassic age of 164.4 ± 36.1 Ma (P2, 49% data) (Figure S9; Table S2). The younger population is younger than the corresponding stratigraphic age (~100–94 Ma; P. Wang et al., 2016), possibly suggesting partially resetting of the AFT system after the deposition. Almost all apatite grains were plotted in the 'HM' and 'I + M' fields of the SVM apatite classification diagram (Figure S9).

3.2.4 Early Jurassic volcanic rocks

Samples B17 and B18 were collected from the Early Jurassic welded tuffs of the Ningyuancun Formation (Figure S1). Sample B17 yielded Middle Jurassic AFT central age (164 ± 7 Ma, Figure S9), younger than its zircon U-Pb age (179 ± 1 Ma, Figure S8), with an insufficient MTL distribution of 12.5 ± 1.2 μm. It possibly implies slightly annealing since then. Samples B18 yielded Early Jurassic AFT central ages (174 ± 9 Ma, Figure S9) overlapping within error with the corresponding zircon U-Pb ages (182 ± 2 Ma, Figure S8), with a MTL of 12.3 ± 1.3 μm (Table S2). This AFT age constrains the timing of magmatic crystallization (Malusà & Fitzgerald, 2020), indicative of no significant annealing due to burial or other reheating event. All apatite grains cluster in the 'I+M' and 'ALK' regions in the SVM apatite classification diagram (Figure S9).

4. A brief summary of zircon U-Pb and Hf isotope, apatite FT and TE compositions data of mid-Cretaceous Songliao Basin

4.1 Syn-rift stage (Shahezi and Yingcheng Formations)

Shahezi Formation

Samples S26–S32 are from the third or fourth member of Shahezi Fm. (SK-IIE well) at the Xujiaweizi Graben (Figure 2). Most of zircons show oscillatory growth zoning with relatively high

Th/U ratios, suggesting a magmatic origin (An, 2018; Song et al., 2022; Yu et al., 2020). These samples consistently reveal a major Early Cretaceous age group at ~130–110 Ma, two secondary age groups at ~190–150 Ma and ~250–210 Ma and a weak age group at ~330–280 Ma (Figure 2). Sample S26 has a juvenile magmatic origin inferred by Hf isotopic analysis (Song et al., 2022). Sample S25 was also collected from the Shahezi Fm. at the south uplift region. Most of zircons are derived from the magmatic origin characteristic of clear oscillatory zones, and define a dominant age group at ~130–110 Ma, and two minor groups at ~170–140 Ma and ~260–230 Ma (Figure 2) (Cheng, 2019).

Yingcheng Formation

Samples S20 and S21 were collected from the Yingcheng Fm. that outcropped at the northeastern and southeastern basin margin, respectively. Most of zircons in sample S21 are derived from the magmatic origin (Figure S5) and yielded a dominant age group at ~200–160 Ma, with minor groups at ~120–110 Ma and ~310–280 Ma (Figure 2). Sample S21 yielded two AFT age populations at ~89 Ma (77% data) and ~179 Ma (23% data)(Figures 3e and S9; Table S2). However, these zircons in sample S20 showed a clear magmatic origin and a unimodal signature at ~230–190 Ma (Figure 2), and its Hf signature from all 10 grains analyzed is juvenile (Song et al., 2022).

Samples S24, S23 and S22 were collected from the Changling, Lishu and Xujiaweizi Grabens, respectively (Figure 2). Sample S24 yielded two major age groups at ~200–160 Ma and ~280–240 Ma, whereas sample S23 shows a major discrete age group at ~320–240 Ma and a secondary discrete age group at ~210–160 Ma (Figure 2). Sample S22 was also collected from the SK-IIE well at the Xujiaweizi Graben, yielded a similar age pattern with these samples from the Shahezi Fm. and defines three major age groups at ~130–105 Ma, ~190–160 Ma, and ~250–210 Ma, with a weak age group at ~310–280 Ma (Figure 2). Most of zircons are from the juvenile magmatic origin confirmed by the typical magmatic oscillatory zones in CL images, high Th/U ratios and Hf isotope analysis (Song et al., 2022).

4.2 Post-rift stage (Denglouku and Quantou Formations)

Denglouku Formation

Samples S12, S13, S14, and S15 were collected from the Denglouku Fm. that outcropped at the southeastern and northeastern basin margin, respectively (Figure 2). Sample S12 (including three samples) was collected from the lower, middle and upper members of the Denglouku Fm, respectively. and yielded two Mesozoic age groups at ~200–160 Ma and ~270–230 Ma, with two minor groups at

~1.8 Ga and ~2.5 Ga (Figure 2). Sample S13 yielded a similar age spectrum with sample S12 with two major age groups at ~200–160 Ma and ~280–240 Ma, and a minor age group at ~2.5–2.4 Ga (Figure 2). The clear oscillatory growth zonation and high Th/U ratios confirm that most of zircons of two samples are derived from the magmatic origin (S. Li et al., 2012; S. Li, He, & Chen, 2020). Samples S14 and S15 are located at the Bin Graben and almost all zircons are from the magmatic origin and yielded a single age group at ~220–170 Ma (Figures 2 and S5). These apatite fission track ages can be separated into three populations of ~99–85 Ma, ~165–161 Ma and ~334–313 Ma (Figures 3e and S9; Table S2).

Samples S19, S17, S16, and S18 were collected from the south uplift region, Yingshan, and Xujiaweizi Grabens, respectively (Figure 2). Sample S19 was collected from the lower part of the Denglouku Fm. at the south uplift region and yielded two discrete age groups at ~180–120 Ma and ~250–210 Ma (Figure 2). Sample S18 was collected from the second member of the Denglouku Fm. at the Xujiaweizi Graben, and these zircons were derived from the magmatic origin and yielded two major age groups at ~120–100 Ma and ~190–150 Ma (Figure 2) (S. Liu, 2020). Sample S17 was collected from the third member of the Denglouku Fm. at the Yingshan Graben and defines two discrete major age groups at ~150–100 Ma and ~170–150 Ma, with a minor group at ~350–270 Ma (Figure 2). Sample S16 was collected from the fourth member of the Denglouku Fm. at the Yingshan Graben and these zircons yielded four discrete age groups at ~160–120 Ma, ~310–240 Ma, ~2.1–1.6 Ga, and ~2.7–2.3 Ga (Figure 2). In CL images, more than half of these zircon grains show magmatic oscillatory zones, while a considerable proportion of zircons have either a core-rim, or dark and other complicated structures (Song et al., 2022). Hf isotope analyses suggested that Late Paleoproterozoic zircons experienced reworking of pre-existing crust material, while Phanerozoic zircons is hybrid origin between mantle-derived juvenile magmas and crust-derived materials (Song et al., 2022).

Quantou Formation

Samples S1–S6 were collected from the eastern basin margin (Figure 2). Sample S2 was located at the Bin Graben and yielded a dominant age group at ~210–180 Ma and two minor groups at ~120–110 and ~240–220 Ma (Figure 2). Similarly, samples S3 and S4 were collected from the northern Bin Graben and also yielded a dominant age group at ~210–180 Ma with a minor discrete age group at ~530–450 Ma (Figure 2). Most of zircons from three samples are derived from magmatic origin (Figure S5). Sample S2 can be clearly separated into two AFT populations of ~81 Ma (38 % data) and ~162

Ma (62 % data) (Figures 3e and S9; Table S2). Most of these apatite grains were plotted in the ‘I+M’ field, whereas some apatite crystals lying in the ‘LM’ and ‘HM’ fields were also detected (Figure S9). Sample S3 can be statistically decomposed into two age populations at ~80 Ma (51% data) and ~164 Ma (49% data) (Figures 3e and S9; Table S2). Almost all apatite grains were plotted in the ‘HM’ and ‘I + M’ fields in the SVM apatite classification diagram (Figure S9). Most of zircons from sample S1 are also derived from magmatic origin and define a dominant age group at ~190–150 Ma and a minor group at ~230–200 Ma (Figure 2) (T. Li et al., 2021). Samples S5 and S6 from the southeastern basin margin show a considerable proportion of Precambrian zircons with two groups at ~1.8 Ga and ~2.6–2.3 Ga (Figure 2). For the two samples, some zircons displayed oscillatory growth zoning consistent with a primary magmatic origin, while other zircons showed typical fir-tree zoning, sector or planar internal textures (S. Li et al., 2012; S. Li et al., 2020).

Samples S7 and S8 were collected from the south uplift region, whereas samples S9, S10, and S11 were collected from the horst or graben regions in the north basin (Figure 2). Samples S7 and S8 display a dominant magmatic origin and yielded a major age group at ~250–210 Ma and a minor age group at ~130–110 Ma (Figure 2). Sample S10 yielded a unimodal age group at ~130 Ma, whereas sample S11 yielded a major age group at ~150–110 Ma with two secondary age groups at ~190–160 Ma and ~300–270 Ma, and a minor age group at ~240–200 Ma (Figure 2). Sample S9 yielded a major age group at ~150–110 Ma and two secondary age groups at ~1.8 Ga and ~2.5 Ga, with a discrete age range at ~350–210 Ma (Figure 2).

Figure S1

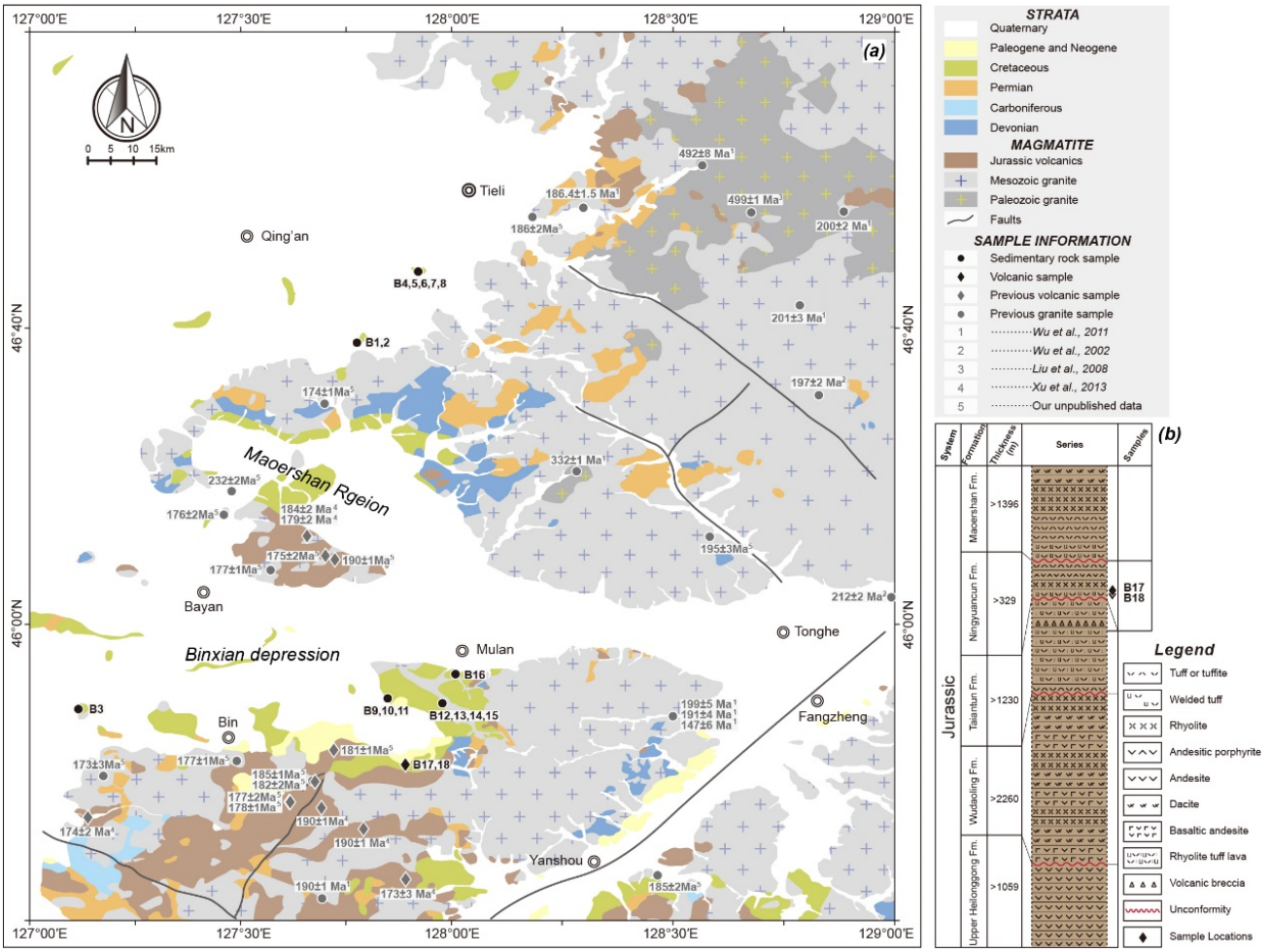

Figure S1 (a) Geological sketch map of northeastern Songliao Basin, showing the spatial distribution of major rock units (Anonymous, 1969, 1970; 1991; and northeast China-related 1:1000000 geological map). The sample locations in this study are also indicated. The previously zircon U-Pb age data for granites and volcanic rocks are sourced from J. Liu et al. (2008); N. Wang et al. (2021); F. Wu et al. (2011); F. Wu, Sun, Li, Jahn, and Wilde (2002); Xu et al. (2013). (b) Stratigraphic column for the Jurassic volcanics in the central Zhangguangcai Range, northeast China, modified from Anonymous (1969, 1970, 1991); Xu et al. (2013).

Figure S2

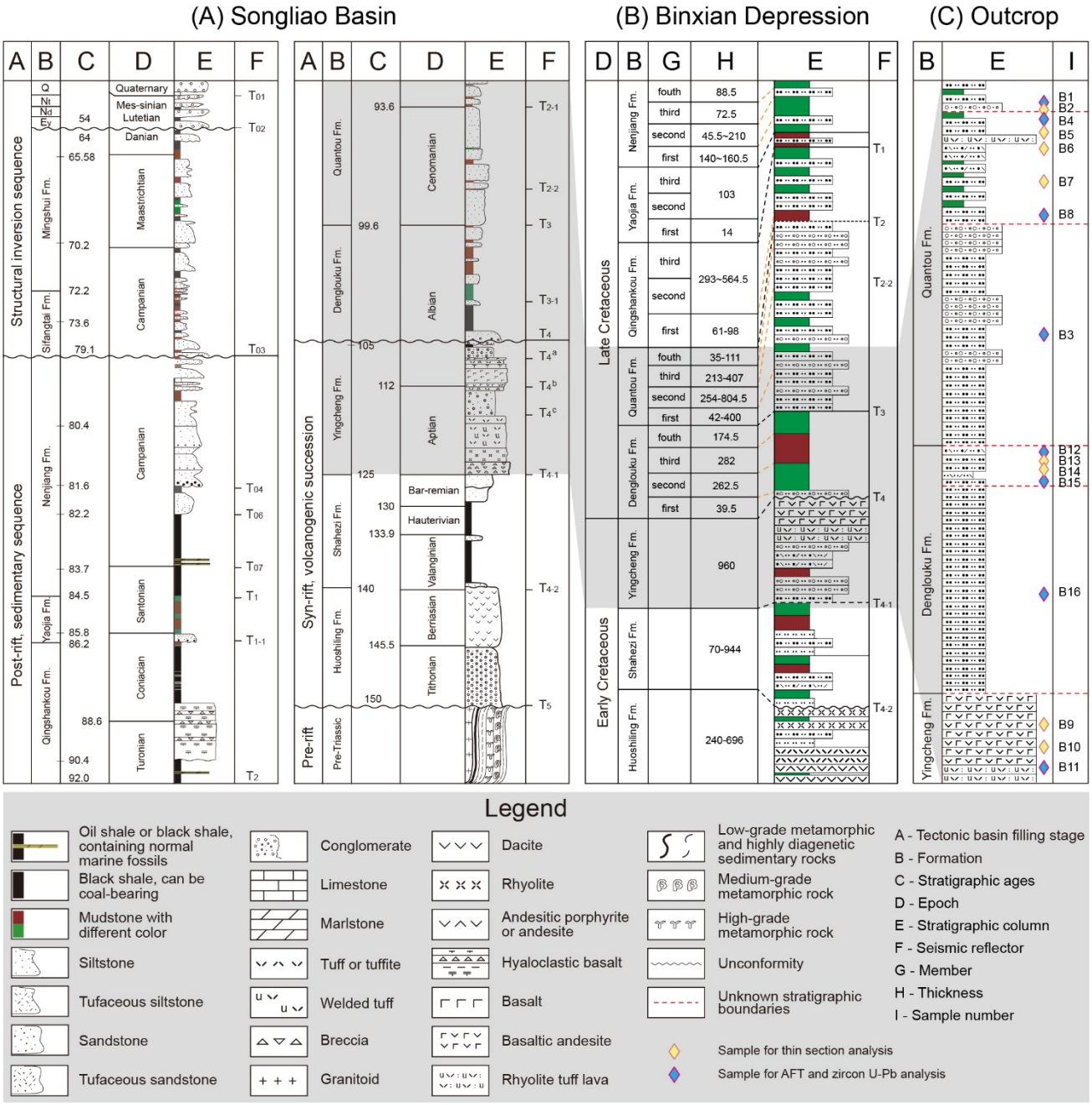

Figure S2 (a) Vertical basin fill sequence of the Songliao Basin, modified after P. Wang et al. (2016). (b) The stratigraphic column of Haerbin-Suihua region in the northeastern Songliao Basin, retrieved after Cui (2007). (c) The stratigraphic column in the study area. These samples analyzed by detrital zircon U-Pb dating analysis are denoted by the blue lozenge, whereas other samples by thin section observation are denoted by the yellow lozenge.

Figure S3

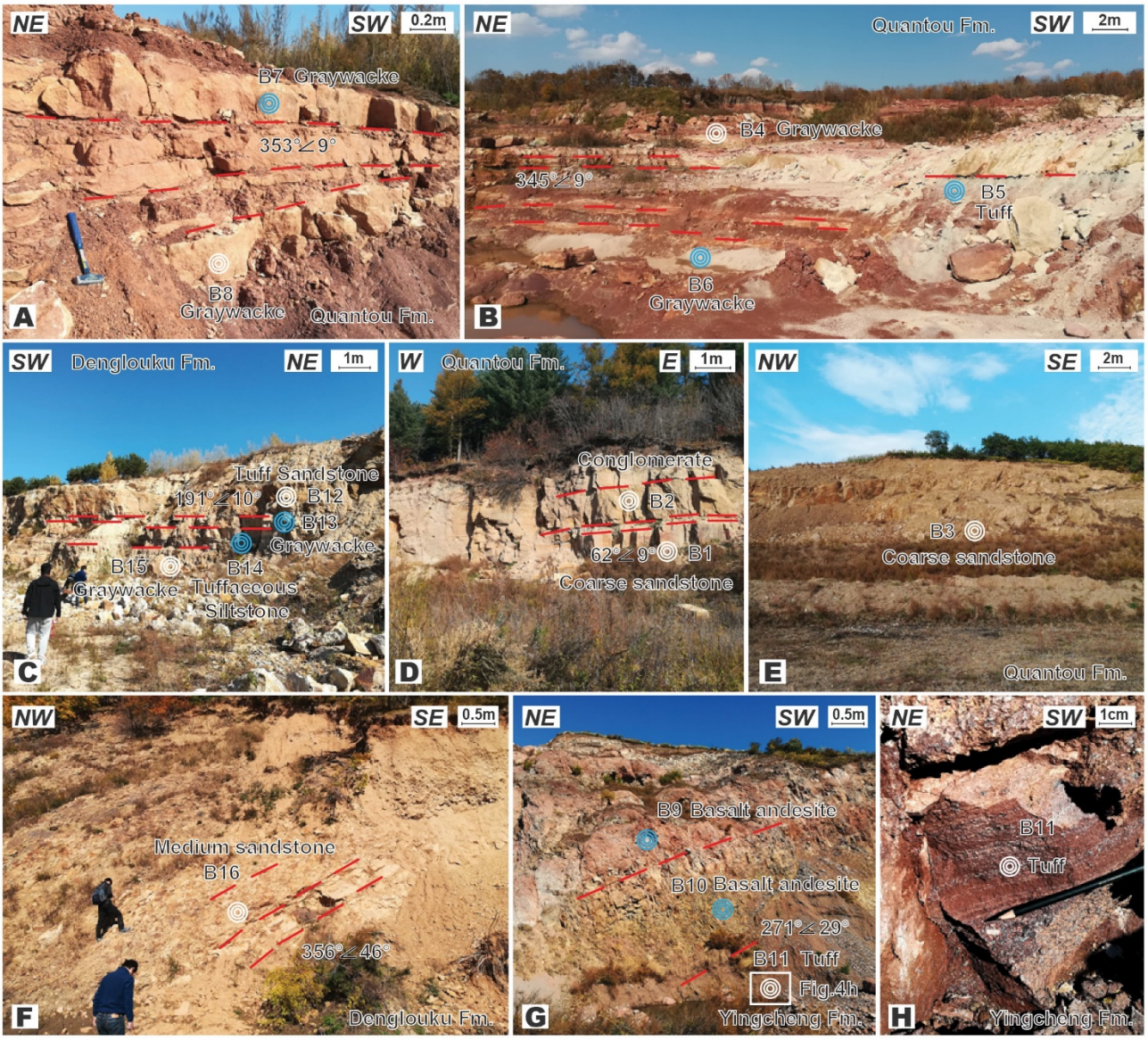

Figure S3 Outcrop photographs showing the main observed lithologies and facies of the sedimentary rocks in the northeastern Songliao Basin, northeast China. (a)–(b) The field outcrop of the Quantou Formation, the upper and lower segments of this formation with the dip direction and dip angle of 345°/9° and 353°/9°, respectively. (d) 62°/9° = dip direction and dip angle of the Quantou Formation. (e) The field outcrop of the Quantou Formation. (c) Dip direction and dip angle of the Denglouku Formation = 191°/10°. (f) 356°/46° = dip direction and dip angle of the Yingcheng Formation. (g)–(h) The field outcrop of the Yingcheng Formation with a dip direction of 271° and dip angle of 29°.

Figure S4

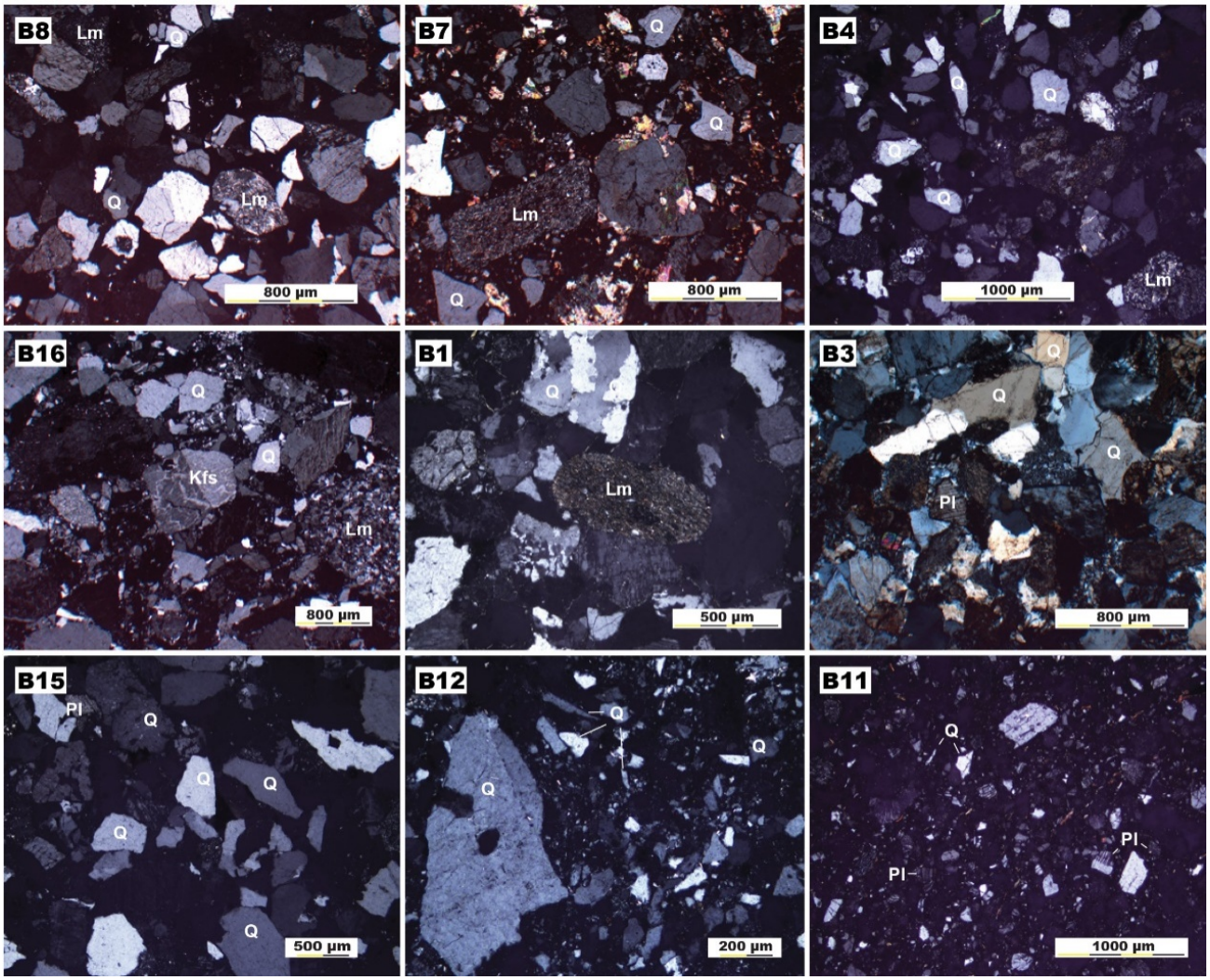

Figure S4 Microscopy photographs (taken under crossed polarizers) displaying petrographic features of sedimentary rocks samples in the northeastern Songliao Basin, northeast China.

Figure S5

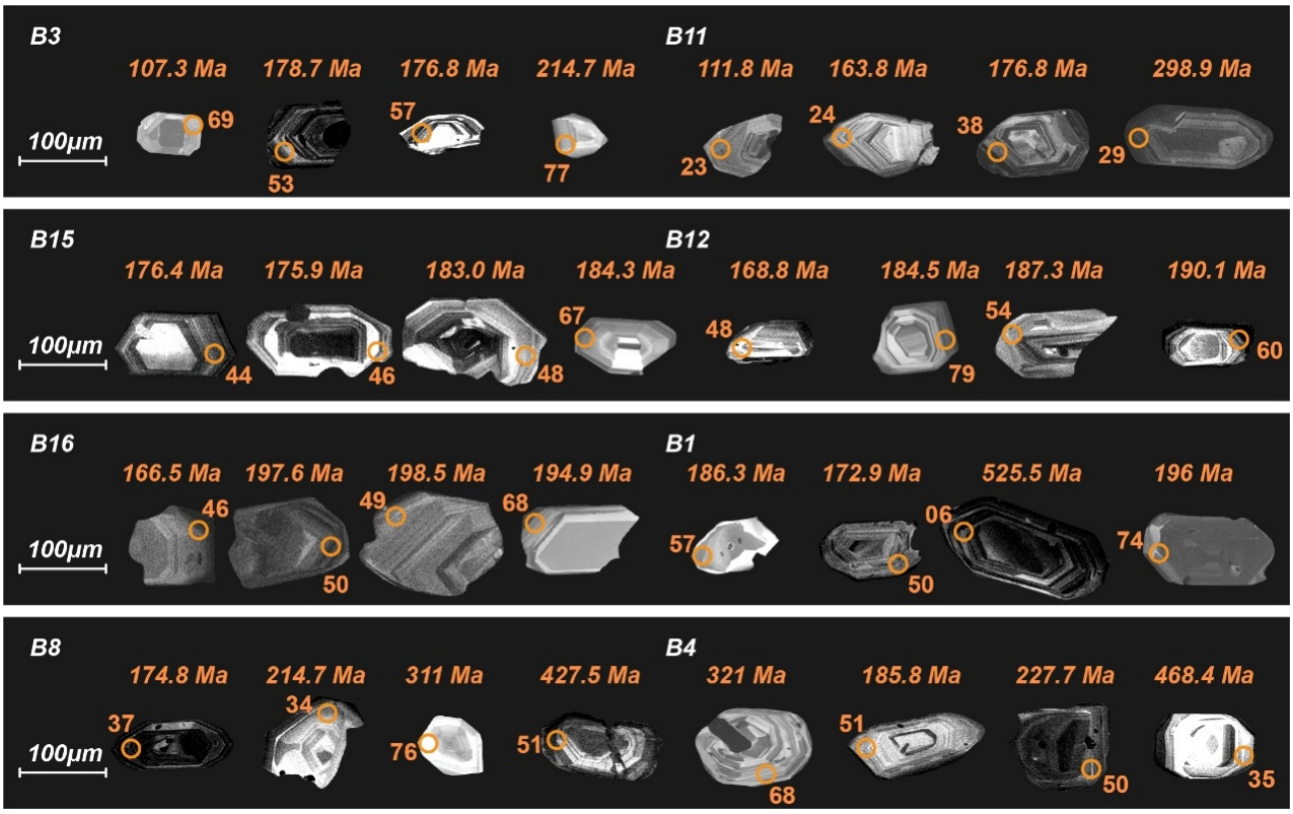

Figure S5 Representative cathodoluminescence (CL) images of zircons from sedimentary rocks in the northeastern Songliao Basin, northeast China. Orange circles indicate the positions of laser spots for age analyses. The sample number (white number), analytical number (orange number), and apparent age (orange number) are also denoted.

Figure S6

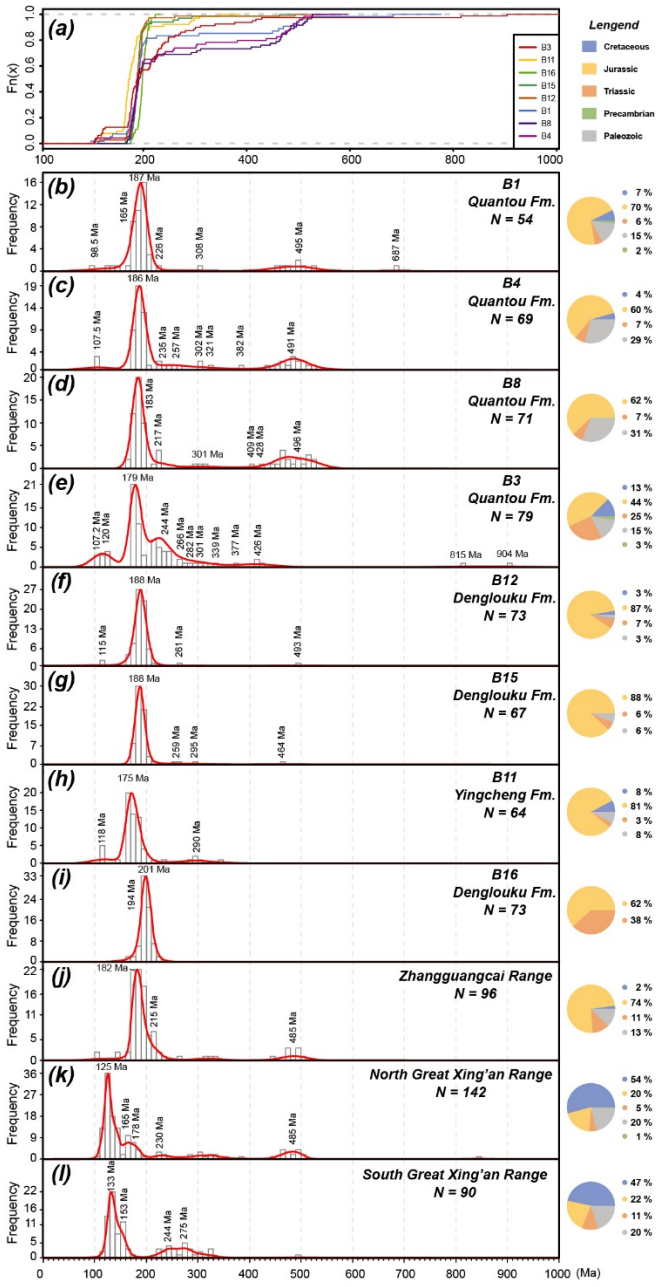

Figure S6 (a) Cumulative zircon U-Pb age distributions for the samples in the northeastern Songliao Basin, northeast China. (b)–(l) Frequency histograms, kernel density estimations and pie charts showing the variation of the samples and different potential provenances in the Songliao Basin, sampling locations seen from Figure S1. For data sources of the potential sources see Supplementary Table 4. Cumulative age distributions for these samples exhibit roughly the same tendency when Fn < 0.6, indicative of no significant change of provenance in study area. However, when Fn > 0.6, these sample slops have relatively differences and could be classified into three groups: B1, B4 and B8; B3; B11, B12, B15 and B16, implying the subtle differences of provenance.

Figure S7

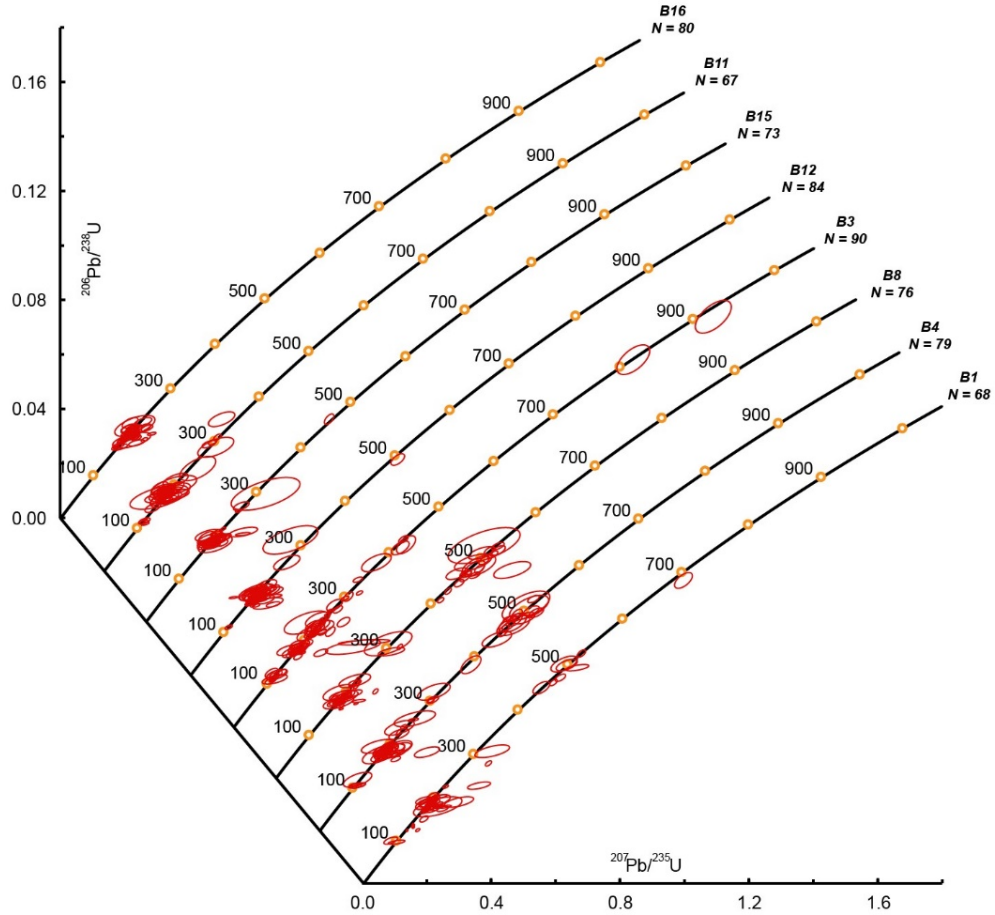

Figure S7 U-Pb concordia diagrams of sedimentary samples collected from the northeastern Songliao Basin, northeastern China. Ages are in Ma and ellipses show 1σ errors. Highly discordant analyses are excluded.

Figure S8

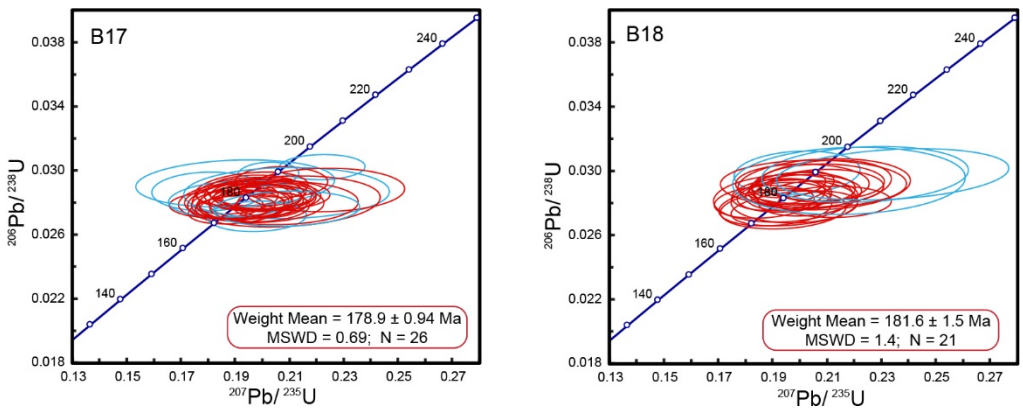

Figure S8 U-Pb concordia diagrams of volcanic rock samples collected from the northeastern Songliao Basin, northeastern China.

Figure S9

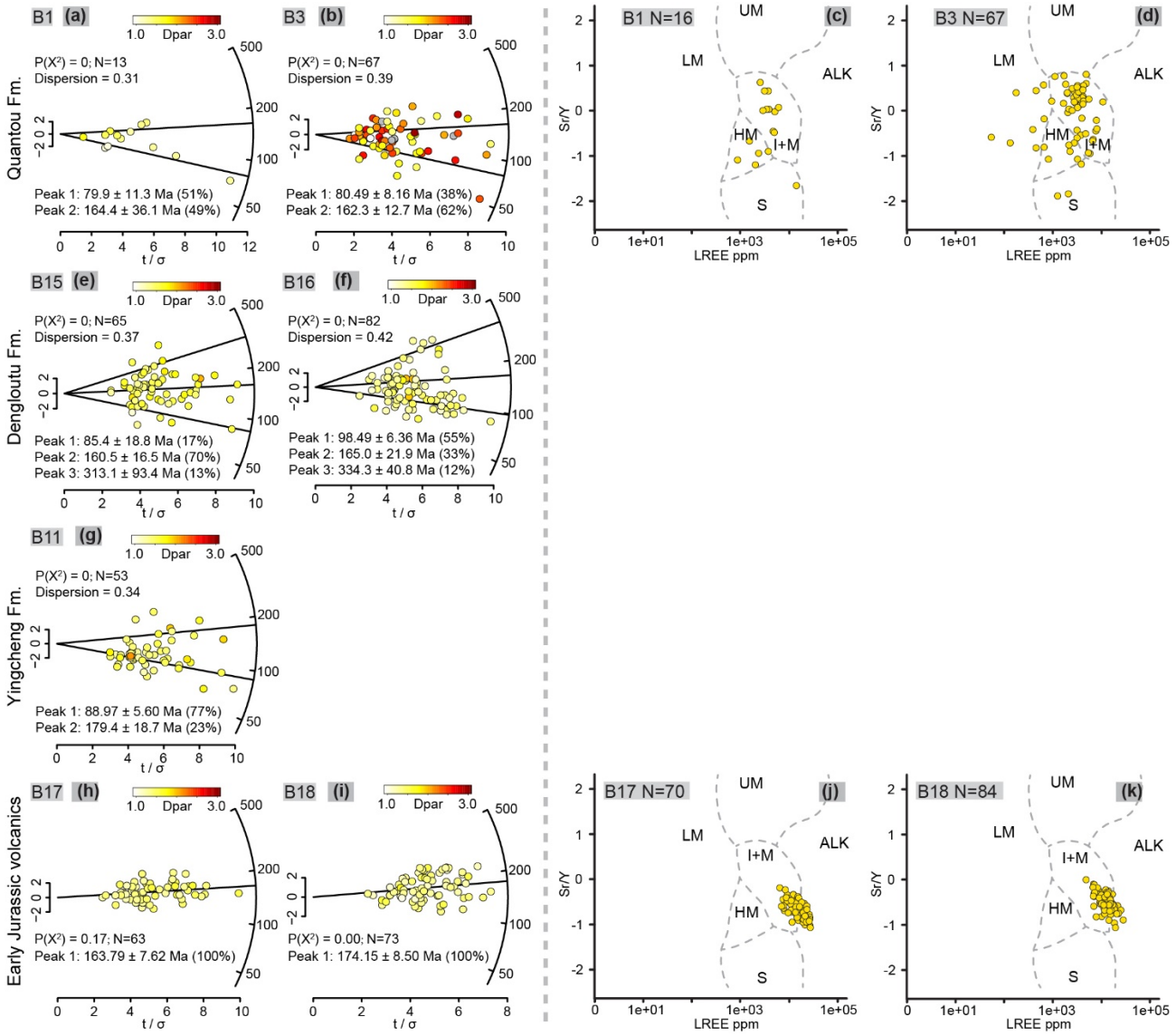

Figure S9 (a)–(b), (e)–(f), (g) and (h)–(i) AFT radial plots for the sedimentary rock and volcanic samples from the northeastern Songliao Basin in this study. The colour of single-grain AFT ages correspond to their D_{par} value (in μm). The black lines indicate statistically AFT population ages decomposed by Isoplot R (Vermeesch, 2018). (c)–(d) and (j)–(k) Support vector machine (SVM) apatite categorization scheme (Sr/Y versus LREE [La, Ce, Pr, Nd]) for the northeastern Songliao Basin apatite detritus. Acronyms for groups on SVM biplots: ALK = alkali-rich igneous rocks; I + M = I-type granitoids and mafic igneous rocks; LM = low- and medium-grade metamorphic and metasomatic; HM = high-grade metamorphic; S = S-type granitoids; UM = ultramafic igneous.

Figure S10

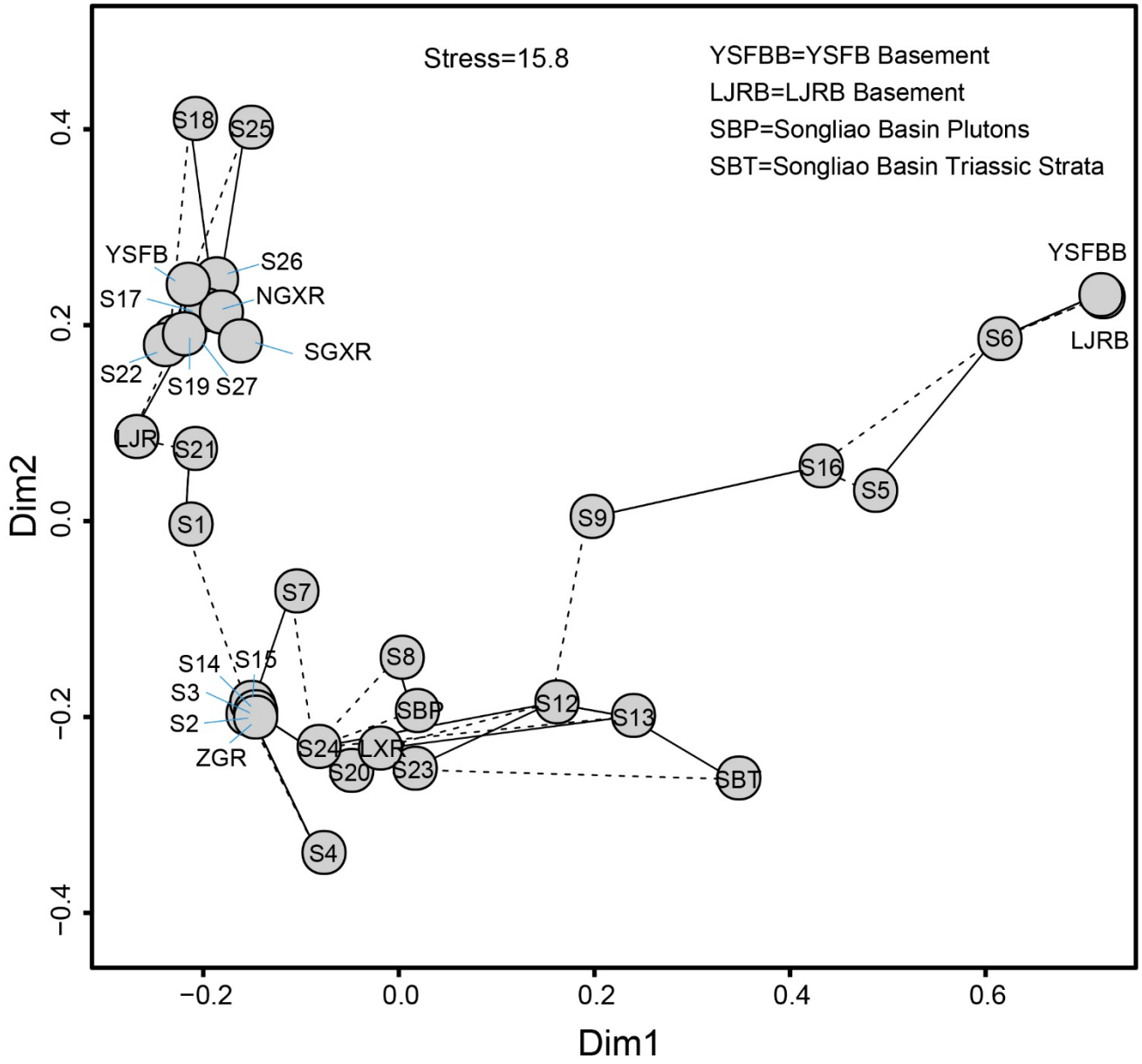

Figure S10 The classic multidimensional scaling plot for zircon U-Pb ages of the Songliao Basin and surrounding potential provenance. ZGR = Zhangguangcai Range. LXR = Lesser Xing'an Range. NGXR = North Great Xing'an Range. SGXR = South Great Xing'an Range. YSFB = Yanshan Fold Belt. LJR = Liaoning-Jilin Region. The solid and dashed lines link the first and second closet neighbors, respectively.

Figure S11

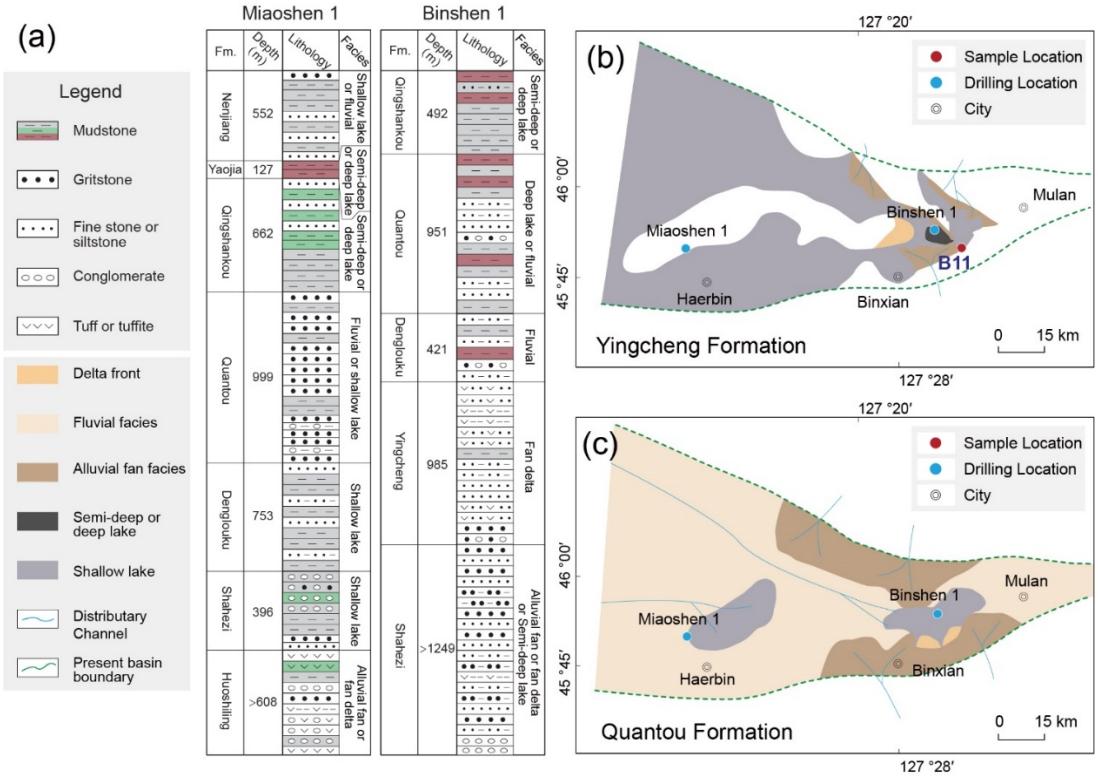

Figure S11 (a) Cretaceous stratigraphy column of the Binxian depression from the Miaoshen 1 and Binshen 1 (Cui, 2007). (b)–(c) Depositional facies map of the Quantou and Yingcheng Formations in the Haerbin-Binxian Depression (Cui, 2007).

Figure S12

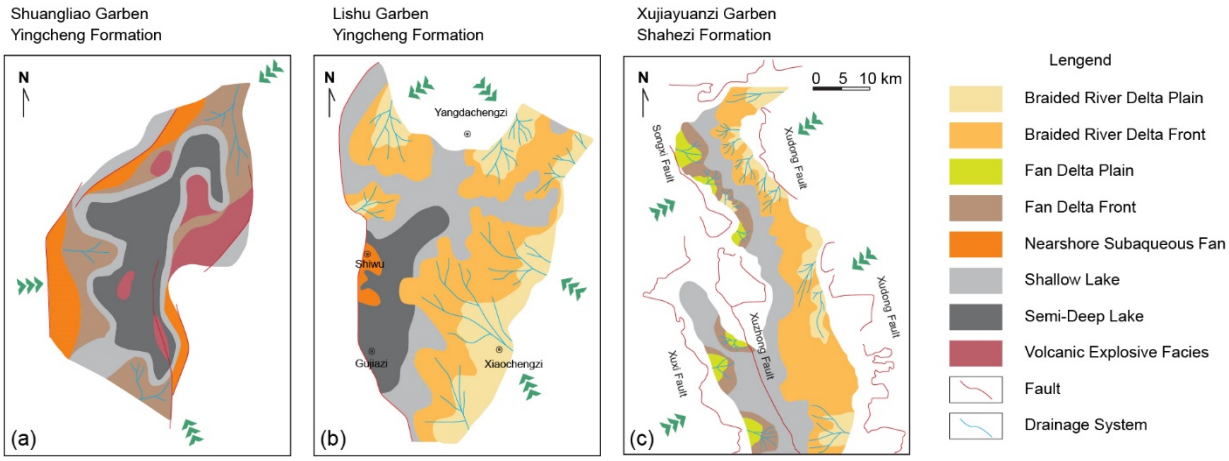

Figure S12 (a) Depositional facies map of the Yingcheng and Shahezi Formations in the Shuangliao, Lishu and Xujiaweizi Grabens (J. Wang, 2017; Yang, Wang, Li, Guan, & Wang, 2021; Zhong & Zhou, 2020).

Figure S13

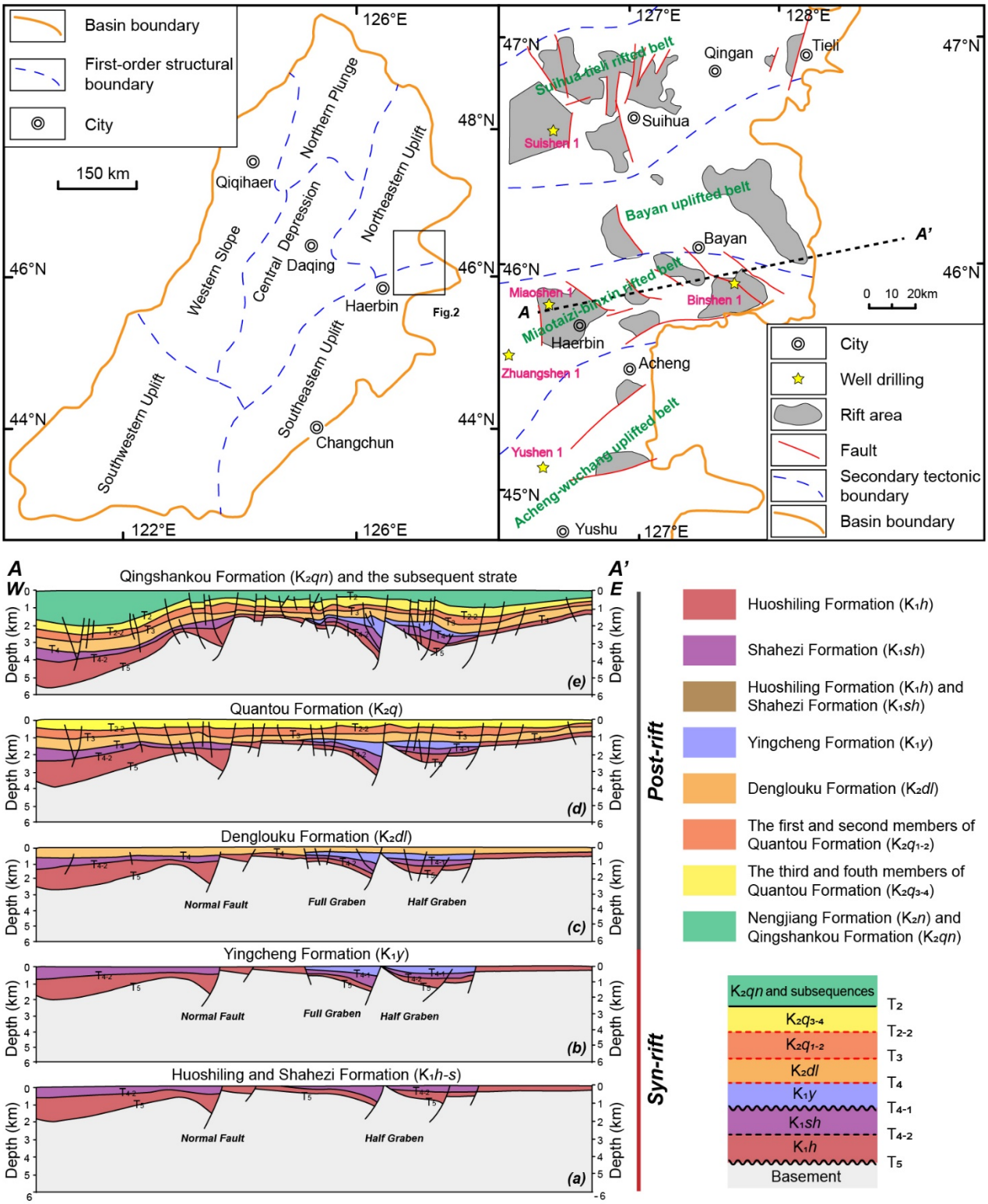

Figure S13 Grabens distribution and tectonic evolution of A-A' seismic reflection profiles in study area exhibiting extension deformation record of the sedimentary rocks during the Early Cretaceous, modified after Cui (2007); Feng et al. (2010).

Figure S14

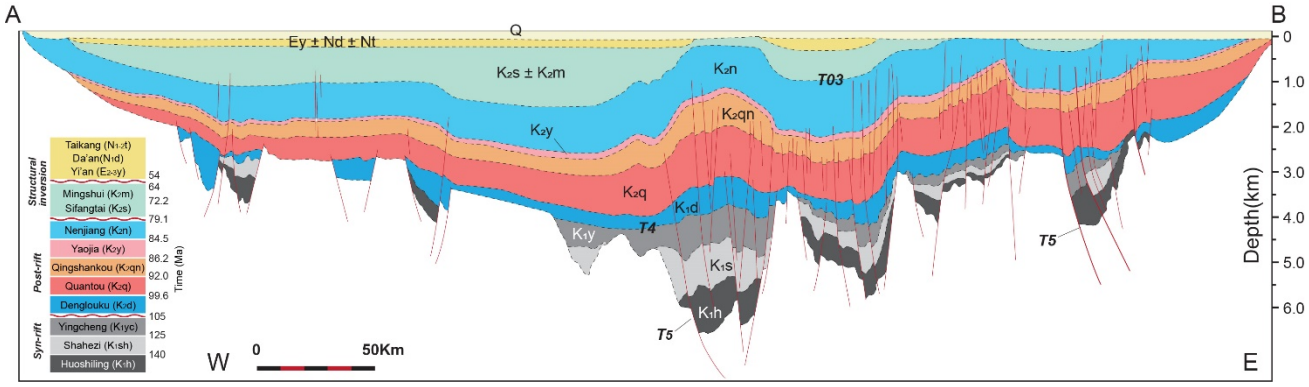

Figure S14 Regional seismic interpreted profile across the northern Songliao Basin reflecting the structure of the basin, modified after P. Wang et al. (2016). See Figure 1c for the section AB location.

Figure S15

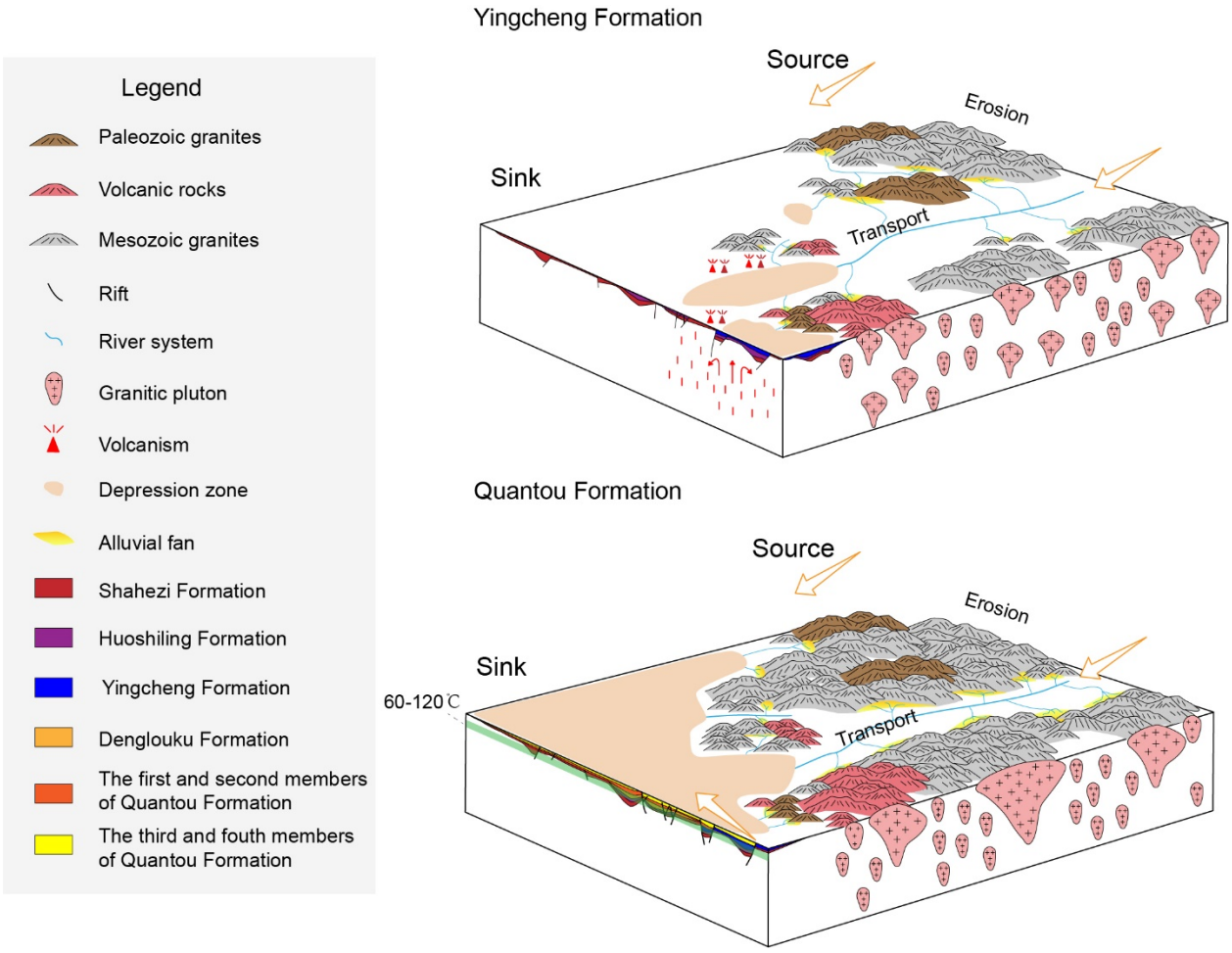

Figure S15 Key period 4D reconstruction of mid-Cretaceous tectonic evolution in the northeastern Songliao Basin, as described in this work.

Figure S16

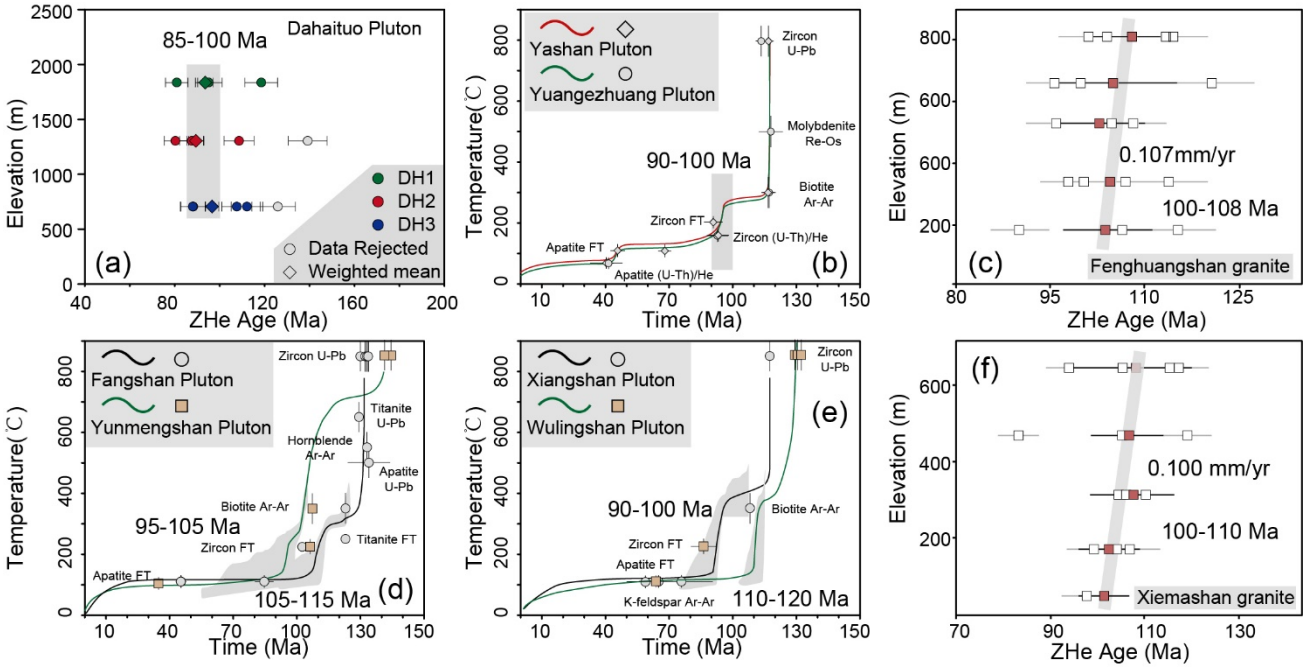

Figure S16 (a), (c) and (f) ZHe age-elevation relationships from Dahaituo plutons of the eastmost YSFB and Fenghuangshan granite and Xiemashan granite of the LJR (Chen, 2019; Y. Wang et al., 2022). (b), (d) and (e) Cooling curves for several plutons from the north NCC (L. Wu et al., 2018; L. Wu et al., 2014). These results consistently reveal an episode of rapid cooling at ~85–110 Ma.

Table S1

Summarized characteristics of samples from the northeastern Songliao Basin, northeast China.

Table S2

Apatite FT data of sedimentary and volcanic rocks samples from the northeastern Songliao Basin, northeast China. No. of grains = number of grains analyzed. ρ_s = spontaneous fission track density. ^{238}U = average uranium concentration. P (χ^2) = the value of chi-squared probability test. P_n = AFT population ages. MTL = mean confined track length. N_L = number of confined track lengths measured.

Table S3

Summarized information of previous published detrital zircon U-Pb and Hf isotopic samples from the Songliao Basin, northeast China.

Table S4

Summary of axial direction, sedimentary facies and major faults of major grabens from the Songliao Basin, northeast China.

Table S1 Summarized characteristics of samples from the northeastern Songliao basin, northeast China.

Laboratory number	Published number	GPS coordinate	Lithology	Maximum depositional age (Ma)	Major age peaks
Quantou Formation					
18SB-39a	B1	N46° 38' 2" E127° 46' 44"	Coarse sandstone	98.5 ± 2.9 (n=1)	165 Ma (21%) 187 Ma (62%) 495 Ma (15%) 687 Ma (2%)
18SB-39b	B2		Conglomerate		———
18SB-7	B3	N45° 48' 47" E127° 6' 47"	Coarse sandstone	107.2 ± 1.7 (n=5)	116 Ma (15%) 179 Ma (38%) 228 Ma (36%) 349 Ma (9%) 891 Ma (2%)
18SB-40c	B4	N46° 47' 52" E127° 55' 14"	Tuffaceous greywacke	107.5 ± 3.0 (n=3)	103 Ma (5%) 186 Ma (60%) 278 Ma (15%) 491 Ma (20%)
18SB-40d	B5		Tuff		———
18SB-40e	B6		Tuffacous greywacke		———
18SB-40b	B7		Greywacke		———
18SB-40a	B8		Greywacke		183 Ma (59%) 217 Ma (10%) 307 Ma (4%) 496 Ma (27%)
Denglouku Formation					
18SB-19d	B12	N45° 50' 5" E127° 51 ' 17"	Tuffaceous standstone	115.4 ± 2.7 (n=2)	110 Ma (3%) 188 Ma (92%) 250 Ma (2%) 494 Ma (3%)
18SB-19b	B13		Greywacke		———
18SB-19c	B14		Tuffaceous siltstone		———
18SB-19a	B15		Greywacke		188 Ma (88%) 263 Ma (8%) 472 Ma (4%)
18SB-20	B16	N45° 53' 15" E128° 0' 59"	Medium standstone	Unknown	194 Ma (22%) 201 Ma (78%)
Yingcheng Formation					
18SB-18a	B9	N45° 50' 42" E127° 49 ' 33"	Basalt andesite	117.6 ± 4.5 (n=5)	———
18SB-18b	B10		Basalt andesite		———
18SB-18c	B11		Andesitic crystal tuff		116 Ma (5%) 175 Ma (79%) 290 Ma (16%)
Ningyuancun Formation					
19SB-19a	B17	N45° 41' 12" E127° 53' 28"	Welded tuff	178.9 ± 1.0 (n=26)	———
19SB-19b	B18		Welded tuff	181.6 ± 1.5 (n=21)	———

Table S2 Apatite FT data of sedimentary and volcanic rocks samples from the northeastern Songliao basin, northeast China.

Laboratory number	Published number	No. of grains	ρ_s (10^5cm^{-2})	^{238}U (ppm)	Age range (Ma)	P(χ^2)	P1	P2	P3	MTL (μm)	N_L
Quantou Formation (Depositional age: ~96-92 Ma)											
18SB-7	B3	67	7.53	13.29	32 - 327	0.00	80.5 ± 8.2 (38%)	162.3 ± 12.7 (62%)	——	12.65 ± 1.99	14
18SB-39b	B1	13	3.12	7.87	64 - 198	0.00	79.9 ± 11.3 (51%)	164.4 ± 36.1 (49%)	——	——	——
Denglouku Formation (Depositional age: ~ 103-96 Ma)											
18SB-20	B16	82	10.47	17.31	57 - 472	0.00	98.5 ± 6.4 (55%)	165.0 ± 21.9 (33%)	334.3 ± 40.8 (12%)	12.69 ± 1.97	35
18SB-19a	B15	65	12.01	17.26	48- 516	0.00	85.4 ± 18.8 (17%)	160.5 ± 16.5 (70%)	313.1 ± 93.4 (13%)	12.03 ± 2.15	25
Yingcheng Formation (Depositional age: ~ 112-103 Ma)											
18SB-18c	B11	53	6.13	11.69	54-324	0.00	89.0 ± 5.6 (77%)	179.4 ± 18.7 (23%)	——	12.58 ± 1.62	65
Early Jurassic volcanics (Eruption timing: ~ 182-179 Ma)											
19SB-19a	B17	63	7.60	9.31	102 - 286	0.17	163.8 ± 7.6 (100%)	——	——	12.48 ± 1.17	14
19SB-19b	B18	73	8.49	9.83	106 - 282	0.00	174.2 ± 8.5 (100%)	——	——	12.34 ± 1.33	12

Table S3 Summarized information of previous published detrital zircon U-Pb and Hf isotopic samples from the Songliao Basin, northeast China.

New Number	Previous Number	Formation	Lithology	Location	Reference
S01	KLHZK2-3 (including 4 samples)	3rd member, Quantou Fm.	Sandstone	Southeastern Margin	Li et al., 2022, Earth Science (In Chinese with English Abstract)
S02	B3	Quantou Fm.	Coarse sandstone	Bindong Garben	This study
S03	B1	Quantou Fm.	Coarse sandstone	Bindong Garben	This study
S04	B4-B8 (including 2 samples)	Quantou Fm.	Tuffaceous greywacke, Greywacke	Bindong Garben	This study
S05	FK11-75	Quantou Fm.	Fine-grained grayish graywacke	Southeastern Margin	Li et al., 2020, GSA Bulletin
S06	SL0932	Quantou Fm.	Fine-grained sandstone	Southeastern Margin	Li et al., 2012, Gondwana Research
S07	Q2.1	2nd-3rd member, Quantou Fm.	Medium-coarse sandstone	South Uplift	Cheng et al., 2019, Doctor's Dissertation of China University of Geoscience; Wang et al., 2022, Sedimentary Geology
S08	ZC3.5	3rd-4th member, Quantou Fm.	Medium-coarse sandstone	South Uplift	Cheng et al., 2019, Doctor's Dissertation of China University of Geoscience; Wang et al., 2022, Sedimentary Geology
S09	SH-1	Quantou Fm.	Sandstone	Miaotaizi Garben	Zhang et al., 2017, Earth-Science Review
S10	Pu311	4th member, Quantou Fm.	Medium-fine sandstone	Daqing Uplift	Chengzhi Yang, 2014, Doctor's Dissertation of China University of Geoscience
S11	Da2	2nd member, Quantou Fm.	Coarse sandstone	Xujiaweizi Garben	Chengzhi Yang, 2014, Doctor's Dissertation of China University of Geoscience
S12	SL0929; SL0930; SL0931 (including 3 samples)	1st-4th member, Denglouku Fm.	Conglomeratic arkose, Conglomeratic gritstone, Fine-grained sandstone	Southeastern Margin	Li et al., 2012, Gondwana Research
S13	FK11-76	1st-2nd member, Denglouku Fm.	Dark-reddish sandstone	Southeastern Margin	Li et al., 2020, GSAB
S14	FK-11-129-134; B12; B15 (including 8 samples)	Denglouku Fm.	Graywacke, Arkose, Conglomeratic ritstone, Fine-grained sandstone, Tuffaceous standstone, Greywacke	Bindong Garben	Li et al., 2020, GSAB and this study
S15	B16	Denglouku Fm.	Medium standstone	Bindong Garben	This study
S16	SLONR29	4th member, Denglouku Fm.	Coarse-grained sandstones to conglomerates	Xujiaweizi Garben	Song et al., 2022, Geoscience Frontiers
S17	W-1	3rd member, Denglouku Fm.	Sandstone	Xujiaweizi Garben	Zhang et al., 2017, Earth-Science Review
S18	SK2	2nd member, Denglouku Fm.	Medium standstone	Xujiaweizi Garben	Suo Liu, 2020, Master's Dissertation of Jilin University
S19	ZC3.3	1st-2nd member, Denglouku Fm.	Medium-coarse sandstone	South Uplift	Cheng et al., 2019, Doctor's Dissertation of China University of Geoscience; Wang et al., 2022, Sedimentary Geology
S20	YC2	2nd member, Yingcheng Fm.	Coarse-grained sandstones to conglomerates	Southeastern Margin	Song et al., 2022, Geoscience Frontiers
S21	B11	Yingcheng Fm.	Andesitic crystal tuff	Bindong Garben	This study
S22	SY8	3rd member, Yingcheng Fm.	Coarse-grained sandstones to conglomerates	Xujiaweizi Garben	Song et al., 2022, Geoscience Frontiers
S23	CL28B-C (including 4 samples)	Yingcheng Fm.	Sandstone-Conglomerate	Lishu Garben	Guanjie Zhang, 2018, Master's Dissertation of Jilin University
S24	CL28A (including 2 samples)	Yingcheng Fm.	Sandstone-Conglomerate	Changling Garben	Guanjie Zhang, 2018, Master's Dissertation of Jilin University
S25	ZC3.4	Shahezi Fm.	Medium-coarse sandstone	South Uplift	Cheng et al., 2019, Doctor's Dissertation of China University of Geoscience; Wang et al., 2022, Sedimentary Geology
S26	S3961	4st member, Shahezi Fm.	Tuff	Xujiaweizi Garben	Yu et al., 2020, Science Bulletin
S27	SY13R1	4st member, Shahezi Fm.	Coarse-grained sandstones to conglomerates	Xujiaweizi Garben	Song et al., 2022, Geoscience Frontiers
S28	DZ01	4st member, Shahezi Fm.	Coarse sandstone	Xujiaweizi Garben	Dongzhao An, 2018, Master's Dissertation of China University of Geoscience
S29	DZ02	4st member, Shahezi Fm.	Coarse sandstone	Xujiaweizi Garben	Dongzhao An, 2018, Master's Dissertation of China University of Geoscience
S30	DZ03	4st member, Shahezi Fm.	Coarse sandstone	Xujiaweizi Garben	Dongzhao An, 2018, Master's Dissertation of China University of Geoscience
S31	DZ04	3rd member, Shahezi Fm.	Coarse sandstone	Xujiaweizi Garben	Dongzhao An, 2018, Master's Dissertation of China University of Geoscience
S32	DZ05	3rd member, Shahezi Fm.	Coarse sandstone	Xujiaweizi Garben	Dongzhao An, 2018, Master's Dissertation of China University of Geoscience

Table S4 Summary of axial direction, sedimentary facies and major faults of major grabens from the Songliao Basin, northeast China.

Number	Graben		Formation	Sedimentary Facies	Major Faults				Reference
	Name	Axial Direction			Name	Strike	Dip Direction	Active Time	
1	Wangfu Graben	SN	Huoshiling	Fan delta front and plain, shallow lake, deep lake, volcanic explosive and volcanic effusive facies	Wangfu Fault	SN	E	T5-T3	Lou, 2019, Doctor's Dissertation of Jilin University
			Shahezi	Fan delta front and plain, shallow lake, deep lake, volcanic explosive and volcanic effusive facies					
			Yingcheng	Fan delta front and plain, shallow lake, deep lake, volcanic explosive and volcanic effusive facies					
2	Zhengsheng Graben	NE	Huoshiling	Fan delta front, shallow lake, sublacustrine fan, volcanic explosive and volcanic effusive facies	Zhengbei Fault	NW	SW	T5-T4	Lou, 2019, Doctor's Dissertation of Jilin University
			Shahezi	Fan delta front, shallow lake, deep lake, sublacustrine fan	Zhengxi Fault	NE	S	T5-T2	
			Yingcheng	Fan delta front and plain, sublacustrine fan, shallow lake, deep lake, and volcanic effusive facies	Zhengdong Fault	NNE	NW	T5-T2	
					Changfa Fault	NNE	NW	T5-T2	
3	Dehui Graben	NNE	Huoshiling	Fan delta front, shallow lake, deep lake, sublacustrine fan and volcanic effusive facies	Nongxi Fault	NNE	SE	T5-T2	Lou, 2019, Doctor's Dissertation of Jilin University
			Shahezi	Fan delta front and plain, shallow lake, deep lake and sublacustrine fan	Longwang Fault	NNE	SE	T5-T2	
			Yingcheng	Fan delta front, shallow lake, deep lake, volcanic explosive and volcanic effusive facies	Dexi Fault	NNE	NW	T5-T4	
					Dedong Fault	NNE	NW	T5-T4	
4	Lishu Graben	SN	Huoshiling	Fan delta front and plain, shallow lake and deep lake, volcanic rock	Sangshutai Fault	SN	E	T5-T3	Lou, 2019, Doctor's Dissertation of Jilin University; Yang et al., 2021, Marine and Petroleum Geology
			Shahezi	Fan delta front and plain, shallow lake and deep lake	Linan Fault	SN	E	T5-T4	
			Yingcheng	Braided river delta plain, front and prodelta, shallow and deep lake	Lidong Fault	SN	E	T5-T4	
			Denglouku	Braided river deposits, braided river delta plain and front, shallow lake	Shuanglong Fault	NE	NW	T5-T4	
5	Shuangliao Graben	NNE	Huoshiling	Nearshore subaqueous fan, fan delta front, shallow lake, volcanic explosive and volcanic effusive facies	Yongjia Fault	NNE	SE	T5-T3	Wang, 2017, Master's Dissertation of Jilin University; Lou, 2019, Doctor's Dissertation of Jilin University
			Shahezi	Nearshore subaqueous fan, fan delta front, shallow lake and deep lake	Shuangxi Fault	SN	E	T5-T3	
			Yingcheng	Nearshore subaqueous fan, fan delta front, shallow lake, deep lake and sublacustrine fan	Shuangdong Fault	SN	SW	T5-T3	
6	Yudong Graben	SN	Huoshiling	Fan delta front, shallow lake, nearshore subaqueous fan, deep lake, volcanic explosive and volcanic effusive facies	Yudong Fault	SN	E	T5-T3	Ren, 2017, Master's Dissertation of Jilin University; Lou, 2019, Doctor's Dissertation of Jilin University
			Shahezi	Fan delta front, shallow lake, deep lake and nearshore subaqueous fan					
			Yingcheng	Fan delta front, nearshore subaqueous fan, shallow lake and deep lake					
7	Yuxi Graben	SN	Huoshiling	Shallow lake, nearshore subaqueous fan and volcanic effusive facies	Yuxi Fault	SN	W	T5-T3	Ren, 2017, Master's Dissertation of Jilin University; Lou, 2019, Doctor's Dissertation of Jilin University
			Shahezi	Shallow lake, deep lake, fan delta front, delta plain and delta front					
			Yingcheng	Fan delta front, fan delta plain, shallow lake and deep lake and volcanic effusive facies					
8	Shanchahe Graben	NE			Shanbei Fault	NW	SW	T5-T4	Lou, 2019, Doctor's Dissertation of Jilin University
					Shannan Fault	NW	NE	T5-T4	
					Shandong Fault	NNE	NW	T5-T3	
					Gongpengzi Fault	NNE	SE	T5-T4	
					Wanfa Fault	NNE	SE	T5-T2	
					Wujiazhan Fault	NE	NW	T5-T4	
9	Xujiaweizi Graben	NNW			Xuxi Fault	NNW	NE		Zhao et al., 2022, Acta Sedimentologica Sinica (In chinese with English abstract)
			Shahezi	Braided delta plain and front, fan delta plain and front, nearshore subaqueous fan, shallow lake and deep lake	Songxi Fault	NNW	NE		
			Huoshiling	Fan delta front and plain, shallow lake and deep lake, volcanic rock					
10	North Changling Graben	NS	Shahezi	Fan delta front and plain, shallow lake					Yang et al., 2021, Marine and Petroleum Geology
			Yingcheng	Braided river delta plain, front and prodelta, shallow and deep lake, volcanic rock					
			Denglouku	Braided river deposits, braided river delta plain and front, shallow lake					
11	Fulong Graben	NE	Huoshiling	Fan delta front and plain, shallow lake and deep lake, nearshore subaqueous fan	Major Fault	NE	NW		Wang et al., 2019, Geoscience
			Shahezi	Fan delta front and plain, shallow lake and deep lake, nearshore subaqueous fan					
			Yingcheng	Fan delta front and plain, shallow lake and deep lake, braided river delta plain and front					
			Denglouku	Braided river delta plain and front, shallow lake and deep lake and sublacustrine fan					
12	Gudian Half-graben	NNW				NNW NE	NEE SE		Wang et al., 2018, Marine and Petroleum Geology
13	Bin Graben		Shahezi	Alluvial fan, fan delta front and plain, shallow lake and deep lake					Cui et al., 2004, Doctor's dissertation of Northwest University
			Yingcheng	Alluvial fan, shallow and deep lake and volcanic rocks					
			Denglouku	Alluvial fan, fan delta front and plain, flood plain, shallow lake and deep lake					
			Quantou	Alluvial fan, flood plain, shallow lake and delta					
14	Sujiatun Graben	NNE	Huoshiling	Fan delta plain and front, shallow lake	Pijia Fault	NE			Deng et al., 2021--Marine and Petroleum Geology
			Shahezi	Fan delta front, shallow and deep lake	Qujia Fault	NS			
			Yingcheng	Braid river dalta plain and front, shallow and deep lake	Sujiatun Fault	NS			

Supplementary Table 1

Data of single-grain zircon U-Pb dating.

Supplementary Table 2

Data of single-grain apatite fission track analysis.

Supplementary Table 3

Data of single-grain apatite trace element.

Supplementary Table 4

Summarized magmatism crystallization ages from the potential provenance surrounding the Songliao Basin.

Supplementary Table 5

Summarized apatite fission track ages data of the basement of the Great Xing'an Range, Zhangguangcai Range and Lesser Xing'an Range.

Supplementary Table 6

Summarized detrital zircon U-Pb ages data of the Shahezi, Yingcheng, Denglouku and Quantou Formations.

Supplementary Table 7

Zircon U-Pb ages of the Songliao Basin basement plutons and strata.

Supplementary Table 8

Zircon U-Pb and Ar-Ar ages of the late Early Cretaceous volcanic rocks in and around the Songliao Basin.

References related to the Precambrian basement of Liao-Ji Region

(Cai et al., 2002; Grant, Wilde, Wu, & Yang, 2009; Hu, Wang, Zhang, Zhao, & Zhang, 2022; S. Li & Zhao, 2007; Z. Li & Chen, 2014, 2019; Z. Li, Chen, & Yan, 2019; F. Liu et al., 2017; F. Liu et al., 2019; J. Liu et al., 2020; Lu, Wu, Zhang, Zhao, & Guo, 2004; Luo et al., 2004; Meng et al., 2014; Meng et al., 2017; Tian et al., 2021; Wan, Song, Yang, & Liu, 2005; Wang, Oh, Lee, & Liu, 2020; Xu et al., 2018; Yuan et al., 2015; H.-F. Zhang et al., 2011; J. Zhang et al., 2020; Zheng, Chen, Liu, & Bao, 2022)

Cai, J., Yan, G., Mu, B., Xu, B., Shao, H., & Xu, R. (2002). U-Pb and Sm-Nd isotopic ages of an alkaline syenite complex body in Liangtun-Kuangdongguo, Gai County, Liaoning Province, China and their geological significance. Acta Petrologica Sinica, 18(3).

Grant, M. L., Wilde, S. A., Wu, F., & Yang, J. (2009). The application of zircon cathodoluminescence imaging, Th–U–Pb chemistry and U–Pb ages in interpreting discrete magmatic and high-grade metamorphic events in the North China Craton at the Archean/Proterozoic boundary. Chemical Geology, 261(1), 155-171. https://doi.org/10.1016/j.chemgeo.2008.11.002

Hu, G., Wang, M., Zhang, S.-H., Zhao, Y., & Zhang, Q.-Q. (2022). A ca. 1.33 Ga mafic dyke identified from the Liaodong Peninsula, northeastern North China Craton: Implications for eastward extension of the Yanliao large igneous province. Precambrian Research, 378, 106770. https://doi.org/10.1016/j.precamres.2022.106770

Li, S., & Zhao, G. (2007). SHRIMP U–Pb zircon geochronology of the Liaoji granitoids: Constraints on the evolution of the Paleoproterozoic Jiao-Liao-Ji belt in the Eastern Block of the North China Craton. Precambrian Research, 158(1), 1-16. https://doi.org/10.1016/j.precamres.2007.04.001

Li, Z., & Chen, B. (2014). Geochronology and geochemistry of the Paleoproterozoic meta-basalts from the Jiao-Liao-Ji Belt, North China Craton: Implications for petrogenesis and tectonic setting. Precambrian Research, 255, 653-667. https://doi.org/10.1016/j.precamres.2014.07.003

Li, Z., & Chen, B. (2019). Lithotectonic elements of Archean basement on the Liaodong Peninsula and its vicinity, North China Craton, China. Frontiers of Earth Science, 13(1), 209-228. doi:10.1007/s11707-018-0708-x

Li, Z., Chen, B., & Yan, X. (2019). The Liaohe Group: An insight into the Paleoproterozoic tectonic evolution of the Jiao–Liao–Ji Belt, North China Craton. Precambrian Research, 326, 174-195. https://doi.org/10.1016/j.precamres.2018.01.009

Liu, F., Liu, C., Itano, K., Iizuka, T., Cai, J., & Wang, F. (2017). Geochemistry, U-Pb dating, and Lu-Hf isotopes of zircon and monazite of porphyritic granites within the Jiao-Liao-Ji orogenic belt: Implications for petrogenesis and tectonic setting. Precambrian Research, 300, 78-106. https://doi.org/10.1016/j.precamres.2017.08.007

Liu, F., Liu, L., Cai, J., Liu, P., Wang, F., Liu, C., & Liu, J. (2019). A widespread Paleoproterozoic partial melting event within the Jiao-Liao-Ji Belt, North China Craton: Zircon U-Pb dating of granitic leucosomes within pelitic granulites and its tectonic implications. Precambrian Research, 326, 155-173. https://doi.org/10.1016/j.precamres.2017.10.017

Liu, J., Zhang, J., Yin, C., Cheng, C., Liu, X., Zhao, C., . . . Wang, X. (2020). Synchronous A-type and adakitic granitic magmatism at ca. 2.2 Ga in the Jiao–Liao–Ji belt, North China Craton: Implications for rifting triggered by lithospheric delamination. Precambrian Research, 342, 105629. https://doi.org/10.1016/j.precamres.2020.105629

Lu, X., Wu, F., Zhang, Y., Zhao, C., & Guo, C. (2004). Emplacement age and tectonic setting of the Paleoproterozoic Liaoji granites in Tonghua area, southern Jilin province. Acta Petrologica Sinica, 20(3), 381-392.

Luo, Y., Sun, M., Zhao, G., Li, S., Xu, P., Ye, K., & Xia, X. (2004). LA-ICP-MS U–Pb zircon ages of the Liaohe Group in the Eastern Block of the North China Craton: constraints on the evolution of the Jiao-Liao-Ji Belt. Precambrian Research, 134(3), 349-371. https://doi.org/10.1016/j.precamres.2004.07.002

Meng, E., Liu, F.-L., Liu, P.-H., Liu, C.-H., Yang, H., Wang, F., . . . Cai, J. (2014). Petrogenesis and tectonic significance of Paleoproterozoic meta-mafic rocks from central Liaodong Peninsula, northeast China: Evidence from zircon U–Pb dating and in situ Lu–Hf isotopes, and whole-rock geochemistry. Precambrian Research, 247, 92-109. https://doi.org/10.1016/j.precamres.2014.03.017

Meng, E., Wang, C.-Y., Li, Y.-G., Li, Z., Yang, H., Cai, J., . . . Jin, M.-Q. (2017). Zircon U–Pb–Hf isotopic and whole-rock geochemical studies of Paleoproterozoic metasedimentary rocks in the northern segment of the Jiao–Liao–Ji Belt, China: Implications for provenance and regional tectonic evolution. Precambrian Research, 298, 472-489. https://doi.org/10.1016/j.precamres.2017.07.004

Tian, Z., Liu, F., Yan, Z., Liu, P., Xu, W., Liu, L., . . . Xiao, W. (2021). Palaeoproterozoic turbidite deposition in the Liaodong Penisula, northeastern North China craton – Constraints from the Gaojiayu formation of the Liaohe Group. Precambrian Research, 352, 106008. https://doi.org/10.1016/j.precamres.2020.106008

Wan, Y., Song, B., Yang, C., & Liu, D. (2005). Zircon SHRIMP U-Pb Geochronology of Archaean Rocks from the Fushun—Qingyuan Area, Liaoning Province and Its Geological Significance. Acta Geologica Sinica, 79(1).

Wang, X., Oh, C. W., Lee, B. C., & Liu, F. (2020). Paleoproterozoic postcollisional metamorphic and igneous activities in the Jinan area of the Jiao-Liao-Ji Belt in the North China Craton and their tectonic implications. Precambrian

Research, 346, 105793. https://doi.org/10.1016/j.precamres.2020.105793

Xu, W., Liu, F., Tian, Z., Liu, L., Ji, L., & Dong, Y. (2018). Source and petrogenesis of Paleoproterozoic meta-mafic rocks intruding into the North Liaohe Group: Implications for back-arc extension prior to the formation of the Jiao-Liao-Ji Belt, North China Craton. Precambrian Research, 307, 66-81. https://doi.org/10.1016/j.precamres.2018.01.011

Yuan, L., Zhang, X., Xue, F., Han, C., Chen, H., & Zhai, M. (2015). Two episodes of Paleoproterozoic mafic intrusions from Liaoning province, North China Craton: Petrogenesis and tectonic implications. Precambrian Research, 264, 119-139. https://doi.org/10.1016/j.precamres.2015.04.017

Zhang, H.-F., Ying, J.-F., Tang, Y.-J., Li, X.-H., Feng, C., & Santosh, M. (2011). Phanerozoic reactivation of the Archean North China Craton through episodic magmatism: Evidence from zircon U–Pb geochronology and Hf isotopes from the Liaodong Peninsula. Gondwana Research, 19(2), 446-459. https://doi.org/10.1016/j.gr.2010.09.002

Zhang, J., Liu, J., Yang, C., Zhang, C., Yang, H., Lu, T., . . . Zhao, L. (2020). Multi-stage Paleoproterozoic structural evolution of the southern Liaodong orogenic belt: A case study of the Hadabei granite gneiss dome. Precambrian Research, 342, 105691. https://doi.org/10.1016/j.precamres.2020.105691

Zheng, J., Chen, B., Liu, S., & Bao, C. (2022). A TRIASSIC OROGENIC GOLD MINERALIZATION EVENT IN THE PALEOPROTEROZOIC METAMORPHIC ROCKS: EVIDENCE FROM TWO TYPES OF RUTILE IN THE BAIYUN GOLD DEPOSIT, LIAODONG PENINSULA, NORTH CHINA CRATON. Economic Geology, 117(7), 1657-1673. doi:10.5382/econgeo.4945

References related to the Precambrian zircon U-Pb ages from the YSFB

(Cai et al., 2002; Chu, Wang, Wei, Liu, & Zhang, 2012; Duan, Wei, & Li, 2019; Duan, Wei, & Qian, 2015; Gao et al., 2009; Gao et al., 2008; Grant, Wilde, Wu, & Yang, 2009; Guo, Sun, Chen, & Zhai, 2005; Han, Wu, Zhou, & Wang, 2020; He, Zhang, Niu, Liu, & Zhao, 2011; Jiang, Guo, Zhai, & Zhang, 2010; Li et al., 2011; D. Liu, Wang, Zhang, & Shi, 2019; H. Liu & Zhang, 2021; J. Liu et al., 2018; S. Liu, Lv, Feng, Liu, et al., 2007; S. Liu, Lv, Feng, Zhang, et al., 2007; S. Liu, Santosh, Wang, Bai, & Yang, 2011; S. Liu, Wang, Bai, Zhang, & Yang, 2010; Lu & Wei, 2020; Qu, Li, & Liu, 2012; Tian et al., 2020; Tian et al., 2015; Wan, Song, Yang, & Liu, 2005; C. Wang, Cui, & KrEner, 1999; F. Wang et al., 2021; W. Wang et al., 2013; W. Wang et al., 2011; W. Wang et al., 2015; Wu, Yang, Zhang, & Liu, 2006; Yan et al., 2005; D. Zhang et al., 2021; H. C. G. Zhang, Zhao, Wang, Yao, & Xu, 2022; S. Zhang, Zhao, Song, & Wu, 2004; S. Zhang, Zhao, Ye, Hu, & Wu, 2013; Zheng, Lu, Yu, & Tang, 2004)

Cai, J., Yan, G., Mu, B., Xu, B., Shao, H., & Xu, R. (2002). U-Pb and Sm-Nd isotopic ages of an alkaline syenite complex body in Liangtun-Kuangdongguo, Gai County, Liaoning Province, China and their geological significance. Acta Petrologica Sinica, 18(3).

Chu, H., Wang, H., Wei, C., Liu, H., & Zhang, K. (2012). The Metamorphic Evolution History of High Pressure Granulites in Chengde Area, Northern Margin of North China: Zircon Chronology and Geochemical Evidence. Acta Geoscientica Sinica, 33(6), 977-987.

Duan, Z., Wei, C., & Li, Z. (2019). Metamorphic P–T paths and zircon u–pb ages of Paleoproterozoic metabasic dykes in eastern Hebei and northern Liaoning: Implications for the tectonic evolution of the North China Craton. Precambrian Research, 326, 124-141. doi.org/10.1016/j.precamres.2017.11.001

Duan, Z., Wei, C., & Qian, J. (2015). Metamorphic P–T paths and Zircon U–Pb age data for the Paleoproterozoic metabasic dykes of high-pressure granulite facies from Eastern Hebei, North China Craton. Precambrian Research, 271, 295-310. doi.org/10.1016/j.precamres.2015.10.015

Gao, L., Zhang, C., LIu, P., Ding, X., Wang, Z., & Zhang, Y. (2009). Recognition of Meso-and Neoproterozoic stratigraphic framework in north and south China. Acta Geologica Sinica, 30(4).

Gao, L., Zhang, C., Yin, C., Shi, X., Wang, Z., Liu, Y., . . . Song, B. (2008). SHRIMP zircon ages: Basis for refining the

Chronostratigraphic classification of the Meso-and Neoproterozoic strata in north China old land. Acta Geoscientica Sinica, 29(3), 366-376.

Grant, M. L., Wilde, S. A., Wu, F., & Yang, J. (2009). The application of zircon cathodoluminescence imaging, Th–U–Pb chemistry and U–Pb ages in interpreting discrete magmatic and high-grade metamorphic events in the North China Craton at the Archean/Proterozoic boundary. Chemical Geology, 261(1), 155-171. doi.org/10.1016/j.chemgeo.2008.11.002

Guo, J. H., Sun, M., Chen, F. K., & Zhai, M. G. (2005). Sm–Nd and SHRIMP U–Pb zircon geochronology of high-pressure granulites in the Sanggan area, North China Craton: timing of Paleoproterozoic continental collision. Journal of Asian Earth Sciences, 24(5), 629-642. doi.org/10.1016/j.jseaes.2004.01.017

Han, S., Wu, C., Zhou, Z., & Wang, G. (2020). Geology, geochemistry, and geochronology of the paleoproterozoic Donggouzi mafic-ultramafic complex: Implications for the evolution of the North China craton. Lithos, 366-367, 105567. doi.org/10.1016/j.lithos.2020.105567

He, Z., Zhang, X., Niu, B., Liu, R., & Zhao, L. (2011). The paleo-weathering mantle of the Proterozoic rapakivi granite in Miyun County Beijing and the relationship with the Changzhougou Formation of Changchengian System. Earth Science Frontiers (China University of Geosciences, Beijing; Peking University), 18(4), 123-130.

Jiang, N., Guo, J., Zhai, M., & Zhang, S. (2010). ~2.7Ga crust growth in the North China craton. Precambrian Research, 179(1), 37-49. doi.org/10.1016/j.precamres.2010.02.010

Li, H., Su, W., Zhou, H., Geng, J., Xiang, Z., Cui, Y., . . . Lu, S. (2011). The base age of the Changchengian System at the northern North China Craton should be younger than 1670 Ma: Constraints from zircon U-Pb LA-MC-ICPMS dating of a granite-porphyry dike in Miyun County, Beijing. Earth Science Frontiers (China University of Geosciences, Beijing; Peking University), 18(3), 108-120.

Liu, D., Wang, X., Zhang, H., & Shi, C. (2019). Zircon SHRIMP U-Pb age of the Chuanlinggou Formation of the Changcheng Group, north China and the stratigraphic implications. Earth Science Frontiers (China University of Geosciences, Beijing; Peking University), 26(3), 183-189.

Liu, H., & Zhang, H.-F. (2021). Chicheng high-pressure granulites record the paleoproterozoic tectonic evolution in the northern North China Craton. Precambrian Research, 359, 106213. doi.org/10.1016/j.precamres.2021.106213

Liu, J., Zhang, J., Liu, Z., Yin, C., Zhao, C., Li, Z., . . . Dou, S. (2018). Geochemical and geochronological study on the Paleoproterozoic rock assemblage of the Xiuyan region: New constraints on an integrated rift-and-collision tectonic process involving the evolution of the Jiao-Liao-Ji Belt, North China Craton. Precambrian Research, 310, 179-197. doi.org/10.1016/j.precamres.2018.03.005

Liu, S., Lv, Y., Feng, Y., Liu, X., Yan, Q., Zhang, C., & Tian, W. (2007). Zircon and monazite geochronology of the Hongqiyingzi complex, northern Hebei, China. Geological Bulletin of China, 26(9), 1086-1100.

Liu, S., Lv, Y., Feng, Y., Zhang, C., Tian, W., Yan, Q., & Liu, X. (2007). Geology and Zircon U-Pb Isotopic Chronology of Dantazi Complex, Northern Hebei Province. Geological Journal of China Universities, 13(3), 484-497.

Liu, S., Santosh, M., Wang, W., Bai, X., & Yang, P. (2011). Zircon U–Pb chronology of the Jianping Complex: Implications for the Precambrian crustal evolution history of the northern margin of North China Craton. Gondwana Research, 20(1), 48-63. doi.org/10.1016/j.gr.2011.01.003

Liu, S., Wang, W., Bai, X., Zhang, F., & Yang, P. (2010). Geological events of Early Precambrian complex in north Chaoyang area, Liaoning Province. Acta Petrologica Sinica, 26(7), 1993-2004.

Lu, H., & Wei, C. (2020). Late Neoarchean or late Paleoproterozoic high-pressure granulite facies metamorphism from the East Hebei terrane, North China Craton? Journal of Asian Earth Sciences, 190, 104195. doi.org/10.1016/j.jseaes.2019.104195

Qu, J., Li, J., & Liu, J. (2012). Geochronological study on the Fenghuangzui complex of Dantazi Group at northern Hebei Province. Acta Petrologica Sinica, 28(9), 2879-2889.

Tian, H., Li, H., Zhang, J., Su, W., Liu, H., Xiang, Z., & Zhong, Y. (2020). SHRIMP U-Pb dating for zircons from the tuff bed of the Mesoproterozoic Gaoyuzhuang Formation in Jixian Section, Tianjin, and its constraints on the Mesoproterozoic bio-environmental events. Geological Survey and Research, 43(2).

Tian, H., Zhang, J., Li, H., Su, W., Zhou, H., Yang, L., . . . Xu, Z. (2015). Zircon LA-MC-ICPMS U-Pb Dating of Tuff from Mesoproterozoic Gaoyuzhuang Formation in Jixian County of North China and Its Geological Significance. Acta Geoscientica Sinica, 36(5), 647-658.

Wan, Y., Song, B., Yang, C., & Liu, D. (2005). Zircon SHRIMP U-Pb Geochronology of Archaean Rocks from the Fushun—Qingyuan Area, Liaoning Province and Its Geological Significance. Acta Geologica Sinica, 79(1).

Wang, C., Cui, W., & KrEner, A. (1999). Zircon evaporation ages and their geological significance from granitoid of the Jianping metamorphic complex, western Liaoning province. Acta Scientiarum Naturalium Universitatis Pekinensis, 35(4).

Wang, F., Peng, P., Chen, C., Hu, H., Huang, D., Chen, F., & Zhai, M. (2021). Petrogenesis and geological significance of the Paleoproterozoic Dushikou metagabbro-diorite in northern Hebei Province. Acta Petrologica Sinica, 37(1), 269-283.

Wang, W., Liu, S., Bai, X., Li, Q., Yang, P., Zhao, Y., . . . Guo, R. (2013). Geochemistry and zircon U–Pb–Hf isotopes of the late Paleoproterozoic Jianping diorite–monzonite–syenite suite of the North China Craton: Implications for petrogenesis and geodynamic setting. Lithos, 162-163, 175-194. doi.org/10.1016/j.lithos.2013.01.005

Wang, W., Liu, S., Bai, X., Yang, P., Li, Q., & Zhang, L. (2011). Geochemistry and zircon U–Pb–Hf isotopic systematics of the Neoarchean Yixian–Fuxin greenstone belt, northern margin of the North China Craton: Implications for petrogenesis and tectonic setting. Gondwana Research, 20(1), 64-81. doi.org/10.1016/j.gr.2011.02.012

Wang, W., Liu, S., Santosh, M., Deng, Z., Guo, B., Zhao, Y., . . . Guo, R. (2015). Late Paleoproterozoic geodynamics of the North China Craton: Geochemical and zircon U–Pb–Hf records from a volcanic suite in the Yanliao rift. Gondwana Research, 27(1), 300-325. doi.org/10.1016/j.gr.2013.10.004

Wu, F., Yang, J., Zhang, Y., & Liu, X. (2006). Emplacement ages of the Mesozoic granites in southeastern part of the western Liaoning province. Acta Petrologica Sinica, 22(2), 315-325.

Yan, D., Zhou, M., Song, H., Liu, D., Wang, Y., Wang, C., & Dong, T. (2005). A geochronological constraint to the Guandi complex, West Hills of Beijing, and its implications for the tectonic evolution Earth Science Frontiers (China University of Geosciences, Beijing; Peking University), 12(2).

Zhang, D., O'Brien, P. J., Schertl, H.-P., Ma, X., Tian, Z., Zhao, L., & Guo, J. (2021). Metamorphic and geochronological evolution of Paleoproterozoic high-pressure ultra-high-temperature pelitic granulite, Chicheng, northern Trans-North China Orogen. Precambrian Research, 361, 106237. doi.org/10.1016/j.precamres.2021.106237

Zhang, H. C. G., Zhao, G., Wang, C., Yao, J., & Xu, N. (2022). Phase equilibria modelling and zircon U-Pb geochronology of Paleoproterozoic mafic granulites from the Chengde Complex, North China Craton. Precambrian Research, 371, 106576. doi.org/10.1016/j.precamres.2022.106576

Zhang, S., Zhao, Y., Song, B., & Wu, H. (2004). The late Paleozoic gneissic granodiorite pluton in early Pre-cambrian high-grade metamorphic terrains near Longhua county in northern Hebei province, north China: result from zircon SHRIMP U-Pb dating and its tectonic implications. Acta Petrologica Sinica, 20(3), 621-626.

Zhang, S., Zhao, Y., Ye, H., Hu, J., & Wu, F. (2013). New constraints on ages of the Chuanlinggou and Tuanshanzi formations of the Changcheng System in the Yan-Liao area in the northern North China Craton. Acta Petrologica Sinica, 29(7), 2481-2490.

Zheng, J., Lu, F., Yu, C., & Tang, H. (2004). Zircon Hf isotope, U-Pb and trace element analysis on granulite xenoliths in Hannuoba basalt: A Record of Early Evolution of the Lower Crust in North China. Chinese Science Bulletin, 49(4).

References related to the AFT data from the Great Xing'an Range, Lesser Xing'an Range and Zhangguangcai Range

(Chen, 2016; Leng et al., 2022; Li and Gong, 2011; Li et al., 2011; Li et al., 2019; Pang et al., 2020; Wang et al., 2021; Wu et al., 2016)

Chen, D., 2016, Mesozoic-Cenozoic tectonic evolution and low temperature thermochronological study of eastern Heilongjiang, NE China: Doctoral Dissertation of Zhejiang University (in Chinese with English abstract).

Leng, Y., Wang, J., and Zheng, D., 2022, Apatite Fission Track Thermochronology of Granite from Duobaoshan Porphyry Cu (Mo) Deposit, Northeast China: Implications for Cooling History and Ore Preservation: Geofluids, v. 2022.

Li, X., and Gong, G., 2011, Late Mesozoic-Cenozoic exhumation history of the Lesser Hinggan Mountains, NE China, revealed by fission track thermochronology: Geological Journal, v. 46, no. 4, p. 277-287.

Li, X., Yang, X., Xia, B., Gong, G., Shan, Y., Zeng, Q., Li, W., and Sun, W., 2011, Exhumation of the Dahinggan Mountains, NE China from the Late Mesozoic to the Cenozoic: new evidence from fission-track thermochronology: Journal of Asian Earth Sciences, v. 42, no. 1, p. 123-133.

Li, Y., Zhang, D., Sun, X., and Lv, C., 2019, Application of apatite fission-track analysis and zircon U-Pb geochronology to study the hydrothermal ore deposits in the Lesser Hinggan Range: Exhumation history and implications for mineral exploration: Journal of Geochemical Exploration, v. 199, p. 141-164.

Pang, Y., Guo, X., Zhang, X., Zhu, X., Hou, F., Wen, Z., and Han, Z., 2020, Late Mesozoic and Cenozoic tectono-thermal history and geodynamic implications of the Great Xing'an Range, NE China: Journal of Asian Earth Sciences, v. 189, p. 104155.

Wang, N., Zhang, Z., Malusà, M. G., Wu, L., Chew, D., Zhang, J., Xiang, D., and Xiao, W., 2021, Pulsed Mesozoic exhumation in Northeast Asia: New constraints from zircon U-Pb and apatite U-Pb, fission track and (U-Th)/He analyses in the Zhangguangcai Range, NE China: Tectonophysics, v. 818, p. 229075.

Wu, H., Hu, D., Wu, X., You, B., Chang, P., and Zhang, M., 2016, Mesozoic-Cenozoic uplift and denudation of northern Da Hinggan Mountains: Evidence from apatite fission track data: Geological Bulletin of China, v. 35, p. 2058-2062.

References related to the Songliao Basin Triassic strata and plutons

(Gao et al., 2007; Li et al., 2021; Pei et al., 2007; Wu et al., 2000; Yin, 2022; Yin et al., 2019)

Gao, F., Xu, W., Yang, D., Pei, F., Liu, X., and Hu, Z., 2007, LA-ICP-MS zircon U-Pb dating from granitoids in southern basement of Songliao basin: Constraints on ages of the basin basement: Science in China Series D: Earth Sciences, v. 50, no. 7, p. 995-1004.

Li, Z., Chen, J., Zou, H., Wang, C., Meng, Q., Liu, H., and Wang, S., 2021, Mesozoic–Cenozoic tectonic evolution and dynamics of the Songliao Basin, NE Asia: Implications for the closure of the Paleo-Asian Ocean and Mongol-Okhotsk Ocean and subduction of the Paleo-Pacific Ocean: Earth-Science Reviews, v. 218, p. 103471.

Pei, F., Xu, W., Yang, D., Zhao, Q., Liu, X., and Hu, Z., 2007, Zircon U-Pb geochronology of basement metamorphic rocks in the Songliao Basin: Chinese Science Bulletin, v. 52, no. 7, p. 942-948.

Wu, F., Sun, D., Li, H., and Wang, X., 2000, Zircon U-Pb ages of the basement rocks beneath the Songliao Basin, NE China: Chinese Science Bulletin, v. 45, no. 16, p. 1514-1518.

Yin, Y., 2022, Geochronology and Petrology of Triassic basement of the Songliao Basin: implications for regional tectonics Jilin University.

Yin, Y., Gao, Y., Wang, P., Qu, X., and Liu, H., 2019, Discovery of Triassic volcanic-sedimentary strata in the basement of Songliao Basin: Science Bulletin, v. 64, no. 10, p. 644-646.

References related to the late Early Cretaceous volcanic rocks in the Songliao Basin

Chang, W., Shan, X., Yi, J., Du, T. and Qu, Y., 2017. Spatial and temporal distributions of the late Mesozoic volcanic successions and their controlling effects on the Changling fault depression of the Songliao Basin, northeast China. Canadian Journal of Earth Sciences, 54(12): 1194-1213.

Chen, J., Wang, L., Zhang, Y., Ge, W., Yang, H., Ji, Z., Zhang, L. and Tian, D., 2020. Chronological and Geochemical Characterisitics of Volcanic Rocks of the Yingcheng Formation in the Southern Songliao Basin: Constraints on the Early Cretaceous Evolution of the Songliao Basin. Acta Geologica Sinica-English Edition, 94(4): 1276-1300.

Ding, R., Shu, P., Ji, X., Qu, Y., Cheng, R. and Zhang, B., 2007. SHRIMP zircon U-Pb age and geological meaning of reservoir volcanic rocks in Qingshen gas field of the Songliao Basin, NE China. Journal of Jilin University (Earth Science Edition), 37(3)(In Chinese with English Abstract).

Gao, Y., 2007. Chronology and geochemistry of Mesozoic volcanic rocks in southeastern Songliao Basin. The Master's Dissertation of Jilin University (In Chinese with English Abstract).

Hu, C., 2013. Structural characteristics and post-Cretaceous tectonic evolution of the Changling Rift. Oil and Gas Geology (In Chinese with English Abstract).

Huang, Q., Wu, H., Wan, X., He, H. and Deng, C., 2011. New progress of integrated chronostratigraphy of the Cretaceous in Songliao Basin. Journal of Stratigraphy, 35(3) (In Chinese with English Abstract).

Ji, Z., Meng, Q.-a., Wan, C.-b., Ge, W.-C., Yang, H., Zhang, Y.-l., Dong, Y. and Jin, X., 2019. Early Cretaceous adakitic lavas and A-type rhyolites in the Songliao Basin, NE China: Implications for the mechanism of lithospheric extension. Gondwana Research, 71: 28-48.

Jin, X., Ge, W., Xue, Y. and Jin, Y., 2011. Zircon U--Pb ages and Hf isotopic composition of volcanic rocks from Well Linshen 3 in Songliao Basin. Global Geology, 30(1) (In Chinese with English Abstract).

Li, S.-Q., Yang, Y.-Z., Xie, Q.-L., Wang, Y. and Chen, F., 2015. Age constraints on late Mesozoic lithospheric extension and origin of felsic volcanism in the Songliao basin, NE China. The Journal of Geology, 123(2): 153-175 (In Chinese with English Abstract).

Liu, W., 2014. Age, Geochemistry and Petrogenesis of the Yingcheng Formation from Changling depression in the Songliao Basin. The Master's Dissertation of Jilin University (In Chinese with English Abstract).

Pei, F., Xu, W., Yang, D., Ji, W., Yu, Y. and Zhang, X., 2008. Mesozoic Volcanic Rocks in the Southern Songliao Basin: Zircon U-Pb Ages and Their Constraints on the Nature of Basin Basement. Earth Science–Journal of China University of Geosciences, 33(5) (In Chinese with English Abstract).

Shen, Y., 2012. Pyroclastic rock of Yingcheng Formation in Songliao Basin: Facies, Architecture, Application. The Doctoral Dissertation of Jilin University (In Chinese with English Abstract).

Wang, P., Chen, C. and Liu, H., 2016. Aptian giant explosive volcanic eruptions in the Songliao Basin and northeast Asia: A possible cause for global climate change and OAE-1a. Cretaceous Research, 62: 98-108.

Wang, P., Chen, S., Li, W., Chen, H. and Lang, Y., 2010. Chronology, petrology and geochemistry of the Cretaceous crypto-explosive breccia-bearing volcanic rocks: implications for volcanic reservoir and tectonics of the Songliao Basin, NE China. Acta Petrologica Sinica, 26(1): 33-46 (In Chinese with English Abstract).

Wu, Q., Pu, R., Han, M., Cao, H. and Li, Q., 2010. Zircon LA-ICP-MS U-Pb dating for the volcanic rocks in Changling Depression, and its geological implication. Journal of Mineralogy and Petrology (In Chinese with English Abstract), 30(2): 111-119.

Zhang, F., Chen, H. and Dong, C., 2008. SHRIMP zircon U-Pb geochronology of volcanic rocks and discussion on the geological time of the Yingcheng Formation of the northern Songliao Basin. Journal of Stratigraphy (In Chinese with English Abstract), 32(1).

Zhang, F., Chen, H., Yu, X., Dong, C., Yang, S., Pang, Y. and Batt, G.E., 2011. Early Cretaceous volcanism in the northern Songliao Basin, NE China, and its geodynamic implication. Gondwana Research, 19(1): 163-176.

Zhang, F., Cheng, X., Chen, H., Dong, C., Yu, X., Xiao, J., Xu, Y., Pang, Y. and Shu, P., 2009. Zircon chronological and geochemical constraints on the Late Mesozoic volcanic events in the southeastern margin of the Songliao Basin, NE China. Acta Petrologica Sinica, 25(1): 39-54 (In Chinese with English Abstract).

Zhang, F., Pang, Y., Yang, S., Dong, C., Chen, H. and Shu, P., 2007. Geochronology of zircon SHRIMP, geochemistry and its implication of the volcanic rocks from Yingcheng Formation in depression area, the northern Songliao Basin. Acta Geologica Sinica, 81(9): 1248-1258 (in Chinese with English abstract).

References related to Supporting Information

An, D. (2018). Early Cretaceous Sedimentary records and provenance analysis of the upper member of Shahezi formation in Songliao Basin Master's dissertation of China University of Geosciences.

Anonymous. (1969). Geological Map of the Mulan County Region, China, 1:200,000. The First Regional Geological Survey Team of the Heilongjiang Bureau of Geology (in Chinese).

Anonymous. (1970). Geological Map of the Shanzhancun Region, China, 1:200,000. The Regional Geological Survey Team of the Heilongjiang Bureau of Geology (in Chinese).

Anonymous. (1991). Geological Map of the Bayan Region, China, 1:200,000. The First Regional Geological Survey Team of the Heilongjiang Bureau of Geology and Mineral Resources (in Chinese).

Chen, Z. (2019). Low-temperature Thermochronological Study on the Exhumation Process of Cretaceous Putos in Yanqing-Fengning Area of the Western Yanshan Belt Master's dissertation of China University of Geosciences.

Cheng, Y. (2019). Sedimentary filling and tectonic thermal events since Late Cretaceous in the Songliao Basin. Doctoral Dissertation of China University of Geosciences (in Chinese with English abstract).

Cui, J. (2007). Structural evolution of Haerbin-Suihua area in east Songliao Basin and its control over hydrocarbon formation condition. Doctoral Dissertation of Northwestern University (in Chinese with English abstract).

Feng, Z., Jia, C., Xie, X., Zhang, S., Feng, Z., & Cross, T. A. (2010). Tectonostratigraphic units and stratigraphic sequences of the nonmarine Songliao Basin, northeast China. Basin Research, 22(1), 79-95.

Gleadow, A., Gleadow, S., Belton, D., Kohn, B., Krochmal, M., & Brown, R. (2009). Coincidence mapping - a key strategy for the automatic counting of fission tracks in natural minerals. Geological Society, London, Special Publications, 324, 25-36. doi:10.1144/SP324.2

Guo, C., Zhang, Z., Malusà, M. G., Chew, D., Xiang, D., Wu, L., . . . Xiao, W. (2022). Late Cenozoic topographic growth of the South Tianshan Mountain Range: Insights from detrital apatite fission-track ages, northern Tarim Basin margin, NW China. Journal of Asian Earth Sciences, 234, 105277. doi:https://doi.org/10.1016/j.jseaes.2022.105277

Ji, W.-Q., Wu, F.-Y., Wang, J.-M., Liu, X.-C., Liu, Z.-C., Zhang, Z., . . . Zhang, C. (2020). Early Evolution of Himalayan Orogenic Belt and Generation of Middle Eocene Magmatism: Constraint From Haweng Granodiorite Porphyry in the Tethyan Himalaya. Frontiers in Earth Science, 8. doi:10.3389/feart.2020.00236

Li, S., Chen, F., Siebel, W., Wu, J., Zhu, X., Shan, X., & Sun, X. (2012). Late Mesozoic tectonic evolution of the Songliao basin, NE China: Evidence from detrital zircon ages and Sr–Nd isotopes. Gondwana Research, 22(3), 943-955. doi:https://doi.org/10.1016/j.gr.2012.04.002

Li, S., He, S., & Chen, F. (2020). Provenance changes across the mid-Cretaceous unconformity in basins of northeastern China: Evidence for an integrated paleolake system and tectonic transformation. GSA Bulletin, 133(1-2), 185-198. doi:10.1130/b35660.1

Li, T., Yu, R. a., Wang, T., Yin, D., Si, Q., Zhu, Q., . . . Tu, J. (2021). Geochemical characteristics, detrital zircon age and provenance analysis of Upper Cretaceous Quantou Formation in Kalun Lake area, southeast margin of Songliao Basin. Earth Science.

Liu, J., Chi, X., Dong, C., Zhao, Z., Li, G., & Zhao, Y. (2008). Discovery of Early Paleozoic granites in the eastern Xiao Hinggan Mountains, northeastern China and their tectonic significance. Geological Bulletin of China, 27, 534-

544.

Liu, S. (2020). Demarcation of the boundary between Yingcheng Formation and Denglouku Formation of Lower Cretaceous in the north of Songliao Basin and paleoclimate change — Based on continuous coring data of SK2 Master's Dissertation of Jilin University.

Liu, Y., Gao, S., Hu, Z., Gao, C., Zong, K., & Wang, D. (2009). Continental and oceanic crust recycling-induced melt-peridotite interactions in the trans-north China orogen: U-Pb dating, Hf isotopes and trace elements in zircons from mantle xenoliths. Journal of Petrology, 51(1-2), 537-571. doi:10.1093/petrology/egp082

Malusà, M. G., & Fitzgerald, P. G. (2020). The geologic interpretation of the detrital thermochronology record within a stratigraphic framework, with examples from the European Alps, Taiwan and the Himalayas. Earth-Science Reviews, 201, 103074. doi:https://doi.org/10.1016/j.earscirev.2019.103074

O'Sullivan, G., Chew, D., Kenny, G., Henrichs, I., & Mulligan, D. (2020). The trace element composition of apatite and its application to detrital provenance studies. Earth-Science Reviews, 201, 103044. doi:https://doi.org/10.1016/j.earscirev.2019.103044

O'Sullivan, G. J., Chew, D. M., Morton, A. C., Mark, C., & Henrichs, I. A. (2018). An integrated apatite geochronology and geochemistry tool for sedimentary provenance analysis. Geochemistry, Geophysics, Geosystems, 19(4), 1309-1326. doi:https://doi.org/10.1002/2017GC007343

Paton, C., Hellstrom, J., Paul, B., Woodhead, J., & Hergt, J. (2011). Iolite: freeware for the visualisation and processing of mass spectrometric data. Journal of Analytical Atomic Spectrometry 26, 2508-2518.

Song, Y., Ren, J., Liu, K., Lyu, D., Feng, X., Liu, Y., & Stepashko, A. (2022). Syn-rift to post-rift tectonic transition and drainage reorganization in continental rifting basins: Detrital zircon analysis from the Songliao Basin, NE China. Geoscience Frontiers, 13(3), 101377. doi:https://doi.org/10.1016/j.gsf.2022.101377

Spencer, C. J., Kirkland, C. L., & Taylor, R. J. M. (2016). Strategies towards statistically robust interpretations of in situ U-Pb zircon geochronology. Geoscience Frontiers, 7, 581-589.

Vermeesch, P. (2018). IsoplotR: A free and open toolbox for geochronology. Geoscience Frontiers, 9(5), 1479-1493. doi:https://doi.org/10.1016/j.gsf.2018.04.001

Wang, J. (2017). Petroleum geological characteristic of Huoshiling-Yingcheng Formation in Shuangliao fault depression, Songliao Basin Master dissertation of Jilin University.

Wang, N., Zhang, Z., Malusà, M. G., Wu, L., Chew, D., Zhang, J., . . . Xiao, W. (2021). Pulsed Mesozoic exhumation in Northeast Asia: New constraints from zircon U-Pb and apatite U-Pb, fission track and (U-Th)/He analyses in the Zhangguangcai Range, NE China. Tectonophysics, 818, 229075. doi:https://doi.org/10.1016/j.tecto.2021.229075

Wang, P., Mattern, F., Didenko, N. A., Zhu, D., Singer, B., & Sun, X. (2016). Tectonics and cycle system of the Cretaceous Songliao Basin: an inverted active continental margin basin. Earth-Science Reviews, 159, 82-102.

Wang, Y., Wang, F., Wu, L., Zhang, Z., Shi, W., & Yang, L. (2022). Differential post-mineralization thermal evolution of the Jiaodong and Liaodong Areas, Eastern China: An indicator of regional tectonic activity. Gondwana Research, 103, 502-521.

Wiedenbeck, M., Alle, P., Corfu, F., Griffin, W. L., Meier, M., Oberli, F., . . . Speigel, W. (1995). 3 NATURAL ZIRCON STANDARDS FOR U-TH-PB, LU-HF, TRACE-ELEMENT AND REE ANALYSES. GEOSTANDARDS NEWSLETTER, 19(1), 1-23. doi:10.1111/j.1751-908X.1995.tb00147.x

Wu, F., Sun, D., Ge, W., Zhang, Y., Grant, M. L., Wilde, S. A., & Jahn, B. (2011). Geochronology of the Phanerozoic granitoids in northeastern China. Journal of Asian Earth Sciences, 41(1), 1-30.

Wu, F., Sun, D., Li, H., Jahn, B., & Wilde, S. A. (2002). A-type granites in northeastern China: age and geochemical constraints on their petrogenesis. Chemical Geology, 187(1-2), 143-173.

Wu, L., Monié, P., Wang, F., Lin, W., Ji, W., & Yang, L. (2018). Multi-phase cooling of Early Cretaceous granites on the Jiaodong Peninsula, East China: Evidence from 40Ar/39Ar and (U-Th)/He thermochronology. Journal of Asian

Earth Sciences, 160, 334-347. doi:https://doi.org/10.1016/j.jseaes.2017.11.014

Wu, L., Wang, F., Lin, W., Wang, Q., Yang, L., Shi, W., & Feng, H. (2014). Rapid cooling of the Yanshan Belt, northern China: constraints from $^{40}Ar/^{39}Ar$ thermochronology and implications for cratonic lithospheric thinning. Journal of Asian Earth Sciences, 90, 107-126. doi:https://doi.org/10.1016/j.jseaes.2014.04.017

Xu, W., Pei, F., Wang, F., Meng, E., Ji, W., Yang, D., & Wang, W. (2013). Spatial-temporal relationships of Mesozoic volcanic rocks in NE China: constraints on tectonic overprinting and transformations between multiple tectonic regimes. Journal of Asian Earth Sciences, 74, 167-193.

Yang, X., Wang, H., Li, Z., Guan, C., & Wang, X. (2021). Tectonic-sedimentary evolution of a continental rift basin: A case study of the Early Cretaceous Changling and Lishu fault depressions, southern Songliao Basin, China. Marine and Petroleum Geology, 128, 105068. doi:https://doi.org/10.1016/j.marpetgeo.2021.105068

Yu, Z., He, H., Deng, C., Lu, K., Shen, Z., & Li, Q. (2020). New SIMS U-Pb geochronology for the Shahezi Formation from CCSD-SK-IIe borehole in the Songliao Basin, NE China. Science Bulletin, 65(13).

Zhang, Z., Zack, T., Kohn, B., Malusà, M. G., Wu, L., Rezaeian, M., . . . Xiao, W. (2023). From Tethyan subduction to Arabia-Eurasia continental collision: Multiple geo-thermochronological signals from granitoids in NW Iran. Palaeogeography, Palaeoclimatology, Palaeoecology, 621, 111567. doi:https://doi.org/10.1016/j.palaeo.2023.111567

Zhong, A., & Zhou, X. (2020). Provenance and sedimentary system analysis of the Shahezi Formation in the Xujiaweizi fault depression, Songliao Basin. Acta Sedimentologica Sinica, 38.